RML58C04

184

Copy
RM L58C04

NACA RM L58C04

NACA

RESEARCH MEMORANDUM

EFFECTS OF BOATTAIL AREA CONTOURING AND SIMULATED TURBOJET EXHAUST ON THE LOADING AND FUSELAGE-TAIL COMPONENT DRAG OF A TWIN-ENGINE FIGHTER-TYPE AIRPLANE MODEL (U)

By Willard E. Foss, Jr., Jack F. Runckel,
and Edwin E. Lee, Jr.

Langley Aeronautical Laboratory
Langley Field, Va.

NATIONAL ADVISORY COMMITTEE
FOR AERONAUTICS

WASHINGTON

July 14, 1958

NATIONAL ADVISORY COMMITTEE FOR AERONAUTICS

RESEARCH MEMORANDUM

EFFECTS OF BOATTAIL AREA CONTOURING AND SIMULATED TURBOJET EXHAUST ON THE LOADING AND FUSELAGE-TAIL COMPONENT DRAG OF A TWIN-ENGINE FIGHTER-TYPE AIRPLANE MODEL*

By Willard E. Foss, Jr., Jack F. Runckel,
and Edwin E. Lee, Jr.

SUMMARY

An investigation of a twin-engine fighter-type airplane model has been conducted in the Langley 16-foot transonic tunnel to determine the effect on drag of a fuselage volume addition incorporating streamline contouring and more extensive boattailing of the engine shrouds. The effect of hot exhausts from the turbojet engines was simulated with hydrogen peroxide gas generators using scaled nonafterburning engine nozzles. Afterbody pressure distributions, base drag coefficients, and forces on the fuselage-tail configurations are presented at Mach numbers from 0.80 to 1.05 at angles of attack of 0° and 4° for jet pressure ratios from 1 to 7.

The effect of jet operation on both the basic and modified models was generally to decrease base pressures but to increase most other afterbody pressures and, therefore, to result in an overall decrease in fuselage-tail component drag. The addition of volume to the basic model reduced the base drag coefficient by 0.0010 with the jets off and 0.0018 at a typical cruise operating condition of a jet pressure ratio of 3, a Mach number of 0.85, and an angle of attack of 4°. The overall jet-off reduction in fuselage-tail component drag due to the volume addition was a maximum of 0.0040 at a Mach number of 0.90 for an angle of attack of 4°.

INTRODUCTION

In a National Advisory Committee for Aeronautics study to evaluate the effects of jet exhaust on airplane aerodynamics, loading, and stability, some of the more complex configurations which have the fuselage

*Title, Unclassified.

and tail surfaces extending behind the jet exit have recently been examined (refs. 1, 2, and 3). The special case of the airplane with an overhanging afterbody and twin jet engines has also received some attention (refs. 4 and 5). The large base area associated with two engines operating in the nonafterburning condition with the exit nozzles in the closed position could result in a high base drag which would penalize the range of the airplane. In order to evaluate the overall jet effects on a model of a twin-engine fighter-type airplane with a fuselage overhang, an investigation was conducted through the cruise Mach number range in the Langley 16-foot transonic tunnel by using the hydrogen peroxide jet simulator technique described in reference 6.

In addition to evaluating the jet effects, an effort was made to obtain drag reductions, as well as more favorable jet effects, by improving the overall area distribution and the local fuselage geometry in the region of the wing and boattailed engine shrouds. The model was, therefore, modified by the addition of volume to the fuselage in the region between the maximum total cross-sectional-area station and the engine exit station.

In the present investigation results were obtained for the original and modified configurations with nonafterburning engine nozzles. Tests were conducted at angles of attack of 0° and 4° and at free-stream Mach numbers from 0.80 to 1.05. Jet pressure ratios from no jet flow to 7 were established with a jet temperature of approximately $1,360^\circ$ F. Pressure measurements and forces on the fuselage-tail combination were obtained with the jets operating and not operating. The average Reynolds number, based on wing mean aerodynamic chord, was 5.0×10^6 for the investigation.

SYMBOLS

A area

A_b base area, $A_e - A_j$ (fig. 3), sq ft

C_D fuselage-tail drag coefficient (base drag included), $C_{D,m} + C_{p,i}\left(\frac{A_s}{S}\right) - C_{p,b}\left(\frac{A_s - A_j}{S}\right)$

$C_{D,m}$ $\dfrac{\text{Drag measured by balance}}{q_\infty S}$

$C_{D,b}$ base drag coefficient, $C_{p,b}(A_b/S)$

$\Delta C_{D,j}$ incremental drag coefficient due to jet operation

C_L fuselage-tail lift coefficient, $\frac{L}{q_\infty S}$

$\Delta C_{L,j}$ incremental lift coefficient due to jet operation

C_m fuselage-tail pitching-moment coefficient, $\frac{m}{q_\infty S\bar{c}}$

$\Delta C_{m,j}$ incremental pitching-moment coefficient due to jet operation

C_p pressure coefficient, $\frac{p_l - p_\infty}{q_\infty}$

$\Delta C_{p,j}$ incremental pressure coefficient due to jet operation

$\bar{c}$ basic wing-mean-aerodynamic chord, in.

d diameter, in.

H_2O_2 hydrogen peroxide

L fuselage-tail lift, lb

M_∞ free-stream Mach number

m fuselage-tail pitching moment about $0.286\bar{c}$, in-lb

p static pressure, lb/sq ft

p_t total pressure, lb/ sq ft

q_∞ free-stream dynamic pressure, lb/sq ft

S basic wing area, sq ft

x longitudinal distance from shroud exit, positive rearward, in.

y lateral distance from center line of model, positive to right, looking forward, in.

z vertical distance from jet horizontal center line, positive upward, in.

α angle of attack of fuselage reference line (fig. 2), deg

β boattail angle, deg

ϕ meridian angle at engine base (fig. 7(b)), deg

Subscripts:

b base

e shroud exit

i internal

j jet

l local

s seal

∞ free stream

APPARATUS AND METHODS

Wind Tunnel and Support System

The investigation was conducted in the Langley 16-foot transonic tunnel which is a single-return atmospheric tunnel having a slotted test section and provision for air exchange.

The support system, as shown in figures 1 and 2, consisted of a strut-mounted bifurcate sting which held the model by the wing tips near the center line of the tunnel. The forces and moments of the fuselage-tail combination were measured by an internal strain-gage balance supported from the wing panels, which were an integral part of the support system. In order to provide adequate strength in the support system, the wing span was reduced slightly as shown in figure 2.

Models

The basic configuration for this investigation (figs. 1 and 2) was a model of a swept-wing, fighter-type airplane having twin jet engines and an overhanging fuselage. Physical dimensions of the wing and tail surfaces are given in figure 2. The model was constructed entirely of

steel with the exception of plastic overlays on portions of the wing surfaces and the nose-canopy section.

The wing-root inlets of the model were closed and faired to streamline contours, and the original wing plan form was maintained. The engine nacelles and the adjacent surfaces on the lower portion of the overhanging fuselage were extended to correspond to the installation of a jet engine with a long tail pipe.

The model contained two jet simulator units which were supported internally from the wing panels and independently of the fuselage-tail assembly. These units, similar to those shown in figure 7(a) of reference 6, develop a hot exhaust which closely simulates the exhaust characteristics of a turbojet engine. The nozzle discharge coefficient of these units was 0.95 for the jet pressure ratios presented and indicated typical sonic nozzle operation. (See ref. 6.)

A sponge material was inserted in the clearance gap between the fuselage and the wing panels to prevent air flow through the model and to permit the fuselage-tail assembly to deflect the balance under load. An additional seal was installed in the annulus between the fuselage and each jet simulator at the location shown in figure 3. Because of the high temperatures expected in this region during jet operation ($\approx$1,000° F), these seals were constructed of aluminum and fiber glass sheets. A rubber diaphragm seal was used during a number of tests with the jets inoperative.

For some of the tests the model was modified as described in the following section by adding volume in the form of cast aluminum sections faired into the original fuselage with a putty material. A gap of approximately 1/8 inch between the added sections and the wing was filled with a flexible plastic to allow for the deflection of the fuselage on the wing support.

Method of Modification

Data for the basic configuration showed that the model had low pressures at the engine shroud bases and a relatively high fuselage-tail drag in the subsonic cruise region. A study of this configuration indicated that substantial drag reductions might be accomplished by making alterations to the fuselage and engine shrouds by incorporating the following three drag-reduction principles:

(1) Improvement of the overall area distribution in accordance with the transonic area rule.

(2) Utilization of more extensive local boattailing on the engine shrouds.

(3) Improvement of the fuselage contours at the wing root by streamline contouring.

An inspection of the area diagram of the basic model (fig. 4) revealed a steep slope, conducive to drag, in the region just beyond maximum cross-sectional area, and a region of low slope, indicative of poor pressure recovery, along the engine shrouds. It was reasoned that an area adjustment could be applied to the region between maximum cross-sectional area and the engine exits in order to obtain better pressure recovery over the engine shrouds and at the same time improve the overall area distribution in order to obtain some advantages of the area rule. It was pointed out in reference 7 that transonic drag-rise reductions could be obtained by adding volume to the fuselage to improve the area progression. Reference 8 showed that subsonic drag reductions and delays in drag-rise Mach number may also be obtained from volume additions to the fuselage. The improved area progression for the configuration with boattail area contouring is shown in figure 4.

The engine shrouds on the basic model consisted of a cylindrical section and a boattailed section with a small amount of convergence. (See fig. 3.) The data of references 9 and 10 indicate that higher afterbody and base pressure coefficients can be obtained with shapes having continuous boattailing over the afterbody length, provided certain limits of the ratio of base to maximum diameter are not exceeded. In addition, the references indicate that the jet effects should be more favorable. Therefore, in revising the engine shroud lines the volume addition in this region was contoured to provide continuous curvature over a greater length of the fuselage ahead of the jet exits.

At the wing-fuselage juncture the area addition was distributed along the fuselage in accordance with streamline contouring concepts (refs. 11 and 12). The method of reference 13 was utilized in laying out the wing-fuselage juncture lines for a lift coefficient of 0.2 at a Mach number of 0.82. The resulting cross sections (fig. 5(a)) had a step at the wing trailing edge which was faired out at the end of the shroud. Some local adjustments of the lines were necessary in order to provide smooth fairings between sections, and details of the final shapes are given in figure 5(b). The fairing adjustments at the forward ends of the area addition resulted in an unintentional increase in maximum cross-sectional area (fig. 4). Photographs of the modified configuration are presented in figure 6.

Tests

Tests were conducted in the Langley 16-foot transonic tunnel at angles of attack of 0° and 4° at Mach numbers of 0.80, 0.85, 0.90, 0.95,

1.00, and 1.05 with a corresponding Reynolds number variation from 4.80×10^6 to 5.04×10^6. At each test Mach number and angle of attack, the jet simulator units were operated through a cycle of jet pressure ratios of 1, 3, 5, and 1, where a value of 1 has been assigned to the initial and final nonoperating jet conditions. At the higher Mach numbers (1.00 and 1.05) a jet pressure ratio of 7 was included in the cycle. Separate tests were also made through the Mach number range with the jets not operating, and these data are referred to as jet-off values.

Measurements

The general arrangement of the pressure orifices on the basic and the modified models are shown in figures 7 and 8, respectively. Tables I and II present, for the two configurations, the coordinates of these orifices and the distance of each from the exit station in terms of the exit diameter. Tubing from these orifices was routed through the wing panels and the sting members. As indicated in tables I and II, certain of these tubes were connected to pressure transducers. The electrical signals from these transducers were transmitted through carrier amplifiers to recording oscillographs. This rapid-response instrumentation was used to obtain the data during the operating cycle of the jet-simulator units. The remainder of the orifices were connected to banks of manometer tubes which were photographically recorded at the test condition where the jet pressure ratio was 1. Fuselage internal pressures and jet total pressures and temperatures were also obtained. For the tests with the jets not operating, all pressure data were obtained by using manometer tubes.

Fuselage-tail forces and moments were measured on an internal six-component strain-gage balance, and the model angle of attack was determined with an internal pendulum-type strain-gage attitude indicator (fig. 2).

Accuracy

Based on the accuracy of instruments, calibrations, and readout procedures, the data presented are believed to be accurate to within the following limits:

M_∞	± 0.005
α, deg	± 0.1
C_p	± 0.02

$p_{t,j}/p_\infty$	±0.2
$C_{D,b}$	±0.0003
C_D	±0.0010
C_L	±0.0050
C_m	±0.0010

With the exception of the base drag, these accuracies for the force coefficients pertain only to the data obtained from the jet-off tests. Unfortunately, balance accuracies cannot be estimated for the jet-on tests because of variations in strain-gage outputs due to excessive temperature changes inside the model which resulted from the operation of the jet simulators. The values obtained are believed to be accurate enough, however, to afford at least a qualitative indication of the jet effects on the fuselage-tail forces. All force coefficients are based on the area of the basic wing. (See fig. 2.)

The effect of support-system interference on the data is not precisely known but is believed to be small because of the relatively large distances existing between supporting members and the surfaces of the fuselage-tail component. Shock-induced separation of the flow over the fuselage by waves from the boom nose fairings, or impingement of these waves on the afterbody after reflecting from the tunnel walls, was investigated at supersonic speeds. The boom nose fairings were moved upstream by the addition of cylindrical extensions ahead of the wing tip, and the resulting afterbody pressures were compared to those measured with the basic support system. As was the case with the single-engine model reported in reference 14, the pressure differences were found to be negligible. Although the general level of the pressure data may have been affected slightly by the presence of the support system, any comparison of different model configurations or the jet-off and jet-on data of a given configuration should yield a reasonably accurate indication of the effects of the fuselage modification and the jet operation, respectively. In order to show the size and location of the supporting elements relative to the model, the cross-sectional area of the support system is presented in figure 4.

RESULTS

The results of the investigation are first presented as pressure measurements obtained at the region ahead of the engine exits, the region of the engine base annulus, and the region of the overhanging afterbody. The overall effects of the body modification and jet operation are summarized and presented as force measurements on the fuselage-tail portion of the airplane model. Emphasis is placed on the results for subsonic speeds since the cruising speeds for the airplane are subsonic and since the range is particularly dependent on the drag at Mach numbers between 0.80 and 0.90. Increases in pressure coefficient on the shroud boattail, the base, or the afterbody represent reductions in drag for the configurations because of the rearward sloping surfaces on the rear portions of the airplane.

Pressure measurements with the jets off are presented in figures 9 to 11 for the basic model and in figures 12 to 14 for the modified configuration at constant values of Mach number. The effect of jet operation on the pressure distributions at Mach numbers of 0.80, 0.90, 1.00, and 1.05 is illustrated for the basic model in figures 15 and 16 and for the modified model in figures 17 to 19. Pressure distributions ahead of the shroud exit obtained from manometer measurements are compared in figure 20 for both models. Comparisons of the detailed loading for the two configurations are shown in figures 21 and 22 at the selected subsonic Mach numbers of 0.85 and 0.95 for jet pressure ratios of 1 and 3. The variations with Mach number of the base drag coefficients for the two configurations are presented in figure 23 for the jets off and for a jet pressure ratio of 3. Force measurements on the fuselage-tail combination obtained with the internal strain-gage balance are presented in figures 24 and 25 for the jets off. Drag data for similar complete models are given in figure 26. The incremental effects of the jets on the drag, lift, and pitching-moment coefficients are illustrated in figures 27 and 28.

DISCUSSION

Pressure-Distribution Measurements

Model comparisons with jets off.- Measurements obtained on the engine shroud of the basic model (fig. 9) show an abrupt decrease in pressure just behind the faired step shown in figures 3 and 9. This disturbance and the relatively short boattailed portion of the shrouds (fig. 3) were thought to be responsible for the low level of pressure coefficient in the region of the exits. Since there is a definite

tendency toward pressure recovery over the rearmost portion of the shroud, application of the fairings with a greater extent of boattailing would be expected to produce better pressure recovery at the rear of the engine nacelles. This expectation is confirmed in figure 12 at the lower Mach numbers where, for example, the data for a Mach number of 0.80 generally show continuous pressure recovery along the fairing. At higher speeds, however, local accelerations occurred over regions of the fairing having a high degree of curvature.

Base pressure measurements for the basic configuration presented in figure 10 show that low pressures exist at the base of the engine shrouds at subsonic speeds with the jets off. These low pressures would be expected to form an appreciable contribution to the airplane drag because of the large base areas associated with nonafterburning engine operation during cruise flight. As the angle of attack was increased to 4°, the base pressure coefficients showed a positive increase. Some small peripheral variation of the local base pressure is apparent which is presumably caused by the proximity of the fuselage in the region from about $\phi = 0°$ to $\phi = 120°$. The base pressure data for the modified configuration (fig. 13) show an angle-of-attack variation similar to the basic model but less circumferential variation. A comparison of figures 10 and 13 indicates that an appreciable pressure increase was obtained at subsonic speeds as a result of the fuselage modification. This increase in base pressure can be attributed to the higher pressures obtained near the end of the boattail area contouring.

The afterbody pressure distributions presented for the basic model in figure 11 show a region of generally negative pressures on the underside of the body for about one shroud diameter downstream of the jet at all Mach numbers. This is in contrast to the results of reference 1 for a single-engine configuration with a similar overhanging afterbody where the pressures were positive immediately behind the jet exit. These differences are believed to be caused by the more complicated fuselage geometry in the region of the shroud exits and to the ventilated space around the shrouds of the present model. The afterbody pressures for the modified model (fig. 14) are generally slightly higher than those of the basic model in the region directly behind the shroud exits, but beyond about three shroud diameters downstream the afterbody pressures were generally lower. (See fig. 21(a).)

Effect of twin-jet operation.- Only a meager amount of fast-response instrumentation was available for measurement of pressures on the basic engine shroud; therefore, no jet effects on the basic shroud are presented. The effect of jet operation on the pressure distribution over the boattail area contouring fairings is shown in figure 17. Jet pressure ratios in excess of 3 and 5 at subsonic and supersonic speeds, respectively, were required to produce any appreciable effect on the fairing pressures. In

both cases the jet effects were favorable but appeared to be confined to a smaller region ahead of the base as the free-stream Mach number was increased.

The effect of jet operation on base pressures for the basic model is shown in figure 15. Somewhat greater circumferential variation in pressures was obtained on the points for a jet pressure ratio of 1 during the cycling tests than on corresponding points of the jet-off tests (fig. 10). For the jet-off tests the rubber diaphragms which were inserted in the annulus between the fuselage and each jet simulator to prevent air flow through the base annulus were better pressure seals than those seals used in the cycling tests; therefore, the data of figure 10 are believed to be more representative of the actual conditions. At Mach numbers of 0.90 and above, increasing pressure ratio first causes a decrease in base pressures, and at the highest jet pressure ratios the jet causes the pressures to become more positive than the jet-off values. At jet pressure ratios corresponding to cruise flight, however (2.75, ref. 6, engine A), the jets would have a detrimental effect on base pressures. The nature of the jet effects on the base pressures of the modified configuration (fig. 18) are similar to those noted for the basic model; however, the detrimental jet effect at a pressure ratio of 3 was reduced considerably at subsonic speeds.

The general effect of the jets on the pressure distribution along the afterbody (which is shown for a typical orifice row in figs. 16 and 19 for the basic and modified models, respectively) was to increase the pressures in the region from the exit to about two shroud diameters downstream. At higher speeds this favorable pressure increase generally continued to the rear of the overhang. Beyond two shroud exit diameters downstream of the exit, fewer orifices were available for the modified configuration; therefore, the wavy pressure distribution present at higher pressure ratios with the original model is not apparent on the modified configuration. This wavy distribution appears to be associated with the periodic structure of the jet. The afterbody pressure distributions for the two configurations are compared in figure 21(b) at a jet pressure ratio of 3. Generally somewhat higher pressures are observed for the modified model except at the rearmost portion of the overhang ($\phi = 30^{\circ}$). The jet effects on the afterbody pressures are more clearly illustrated in figure 22 where the incremental pressure coefficients caused by the jet are shown for pressure ratios of 3 and 5. These incremental values were obtained by subtracting the pressure coefficients at a jet pressure ratio of 1 from the jet-on pressure coefficients. Again it can be seen that the jet effects are usually more favorable for the modified configuration.

Base Drag Comparisons

The variations of jet-off base drag with Mach number for both the basic and modified models are compared in figure 23(a). Reductions in base drag coefficient for the model with boattail area contouring occurred at all speeds up to a Mach number of 0.98. This drag decrease was approximately 0.0010 at an angle of attack of 4°. At an angle of attack of 0° a maximum base drag reduction of 0.0015 occurred between Mach numbers of 0.85 and 0.90.

The base drag comparisons of figure 23 show that with the jet simulators operating at a jet pressure ratio of approximately 3, the base drag was increased from jet-off values for both configurations. However, at a Mach number of 0.85 and an angle of attack of 4°, the detrimental effect on the base drag of the modified model is only half that of the basic model. The achievement of more favorable jet effects on base drag by using continuous boattailing ahead of the jet exits is consistent with the results of references 9 and 10 for simple bodies of revolution. At a jet pressure ratio of 3 and an angle of attack of 4° (fig. 23(b)), the base drag coefficient was approximately 0.0018 lower for the modified model than the basic configuration up to a Mach number of 0.95, and smaller reductions occurred over the remainder of the Mach number range.

Incremental base drag coefficients due to jet operation are shown in figure 27 for the Mach number range of interest for cruise flight with this type of airplane. The incremental base drag coefficients for both configurations increased up to a pressure ratio of 3, and this increase indicated that the jets were aspirating the bases in this pressure-ratio range. A further increase in pressure ratio reduced the incremental drag coefficient to approximately the values existing at a jet pressure ratio of 1 as the interaction of the exhaust and external stream became predominant. As indicated previously, jet effects on base drag were less detrimental for the modified model.

Fuselage-Tail Force Measurements

The previously discussed changes in loading over the rear portion of the model fuselage caused by the boattail area contouring might be expected to appear as a reduction in the external drag of the fuselage-tail at subsonic speeds. This overall effect is shown in figure 24 as the variation of fuselage-tail drag coefficient obtained through the Mach number range with the jets off. The drag coefficients for the modified model are substantially lower than those for the basic model at speeds up to a Mach number of 0.95. The reduction in drag coefficient achieved at a Mach number of 0.85 is about 0.0026 at both angles of attack, and the reduction varies from about 0.0017 at a Mach number of 0.80 to 0.0042 at a Mach number of 0.91. The continuous decrease in drag

between these Mach numbers is probably caused by an increase in the effectiveness of the fairing in delaying the formation and reducing the strength of local supersonic flow regions in the vicinity of the wing root. Above a Mach number of 0.95 the fuselage-tail drag coefficient of the modified configuration is higher than that of the basic model because the wing drag is not included in the measurements. Unpublished data have indicated that, when the supersonic flow field envelopes a large portion of the wing as well as the fuselage, a large part of the drag reduction appears as a reduction in wing pressure drag. Tests of the complete model, however, are required to show this fact. Drag reductions at supersonic speeds have been obtained in Wright Air Development Center 10-foot transonic tunnel tests of complete basic and modified models similar in configuration to those of the present investigation. The results (previously unpublished) are presented in figure 26 to provide an approximate indication of the magnitude of the drag improvements which might be expected from the present modified configuration if the wing effects were included in the force measurements.

The results of measurements of the other balance components are shown in figure 25. The boattail area contouring caused only slight changes in lift coefficient but produced a positive pitching-moment increment for the fuselage-tail. Comparisons of figures 9 and 12 suggest that this nose-up increment is probably caused by the slight difference in distribution of pressures on the top and bottom of the fairing.

The incremental fuselage-tail drag resulting from jet operation is presented in figure 27 for both configurations and includes the jet effects on base drag. It may be seen that the fuselage-tail drag decreases with increasing jet pressure ratio even though the jet effects on base drag are generally detrimental.

The incremental lift and pitching-moment coefficients caused by jet operation are shown in figure 28. The slight increases in lift and nose-down pitching moment appear to be caused by the local increases in pressure coefficient along the bottom surface of the overhang with the jets operating.

Although the fuselage-tail incremental drag, lift, and pitching-moment coefficients of figures 27 and 28 were subject to errors of unknown magnitude introduced by balance heating as discussed previously, the variation of the data of these figures with jet pressure ratio generally appears to be consistent with trends indicated by the pressure data.

SUMMARY OF RESULTS

An investigation of the effects of boattail area contouring and simulated turbojet exhaust on the loading and fuselage-tail component drag of a twin-engine fighter-type airplane model having an overhanging afterbody showed the following results pertaining to cruise operating conditions:

1. The low pressures in the vicinity of the engine exits contributed appreciable drag to the basic configuration.

2. The effect of jet operation on both configurations generally was to reduce pressures on the engine bases but to increase pressures on the engine boattails and on the underside of the fuselage overhang and, therefore, to result in an overall decrease in fuselage-tail drag as the jet pressure ratio was increased from 1 to 5.

3. A volume addition to the fuselage, intended to improve the local boattailing, overall area distribution, and wing-root streamlining, reduced the base drag coefficient by about 0.0010 with the jets not operating and approximately 0.0018 at a pressure ratio of 3, a Mach number of 0.85, and an angle of attack of 4°.

4. The overall jet-off reduction in fuselage-tail component drag due to the volume addition ranged from 0.0018 at Mach number of 0.80 to a maximum of 0.0040 at a Mach number of 0.90 for an angle of attack of 4°.

Langley Aeronautical Laboratory,
National Advisory Committee for Aeronautics,
Langley Field, Va., February 19, 1958.

REFERENCES

1. Cornette, Elden S., and Ward, Donald H.: Transonic Wind-Tunnel Investigation of the Effects of a Heated Propulsive Jet on the Pressure Distribution Along a Fuselage Overhang. NACA RM L56A27, 1956.

2. Blanchard, Willard S., Jr.: Free-Flight Investigation of Jet Effect on the Low-Lift Drag and Longitudinal Trim of a Supersonic Interceptor-Type Airplane Configuration With an Overhanging Tail Boom at Mach Numbers From 1.09 to 1.34. NACA RM L57G11, 1957.

3. Jackson, Bruce G.: Free-Flight Transonic Model Investigation of Jet Effects on a Fighter-Type Configuration Employing a Tail Boom and Three Horizontal-Tail Positions. NACA RM L57J31, 1958.

4. Mitcham, Grady L.: A Summary of the Longitudinal and Lateral Stability and Control Characteristics Obtained From Rocket-Model Tests of a Swept-Wing Fighter-Type Airplane at Mach Numbers From 0.5 to 1.9. NACA RM L56K19, 1957.

5. Swihart, John M., and Crabill, Norman L.: Steady Loads Due to Jet Interference on Wings, Tails, and Fuselages at Transonic Speeds. NACA RM L57D24b, 1957.

6. Runckel, Jack F., and Swihart, John M.: A Hydrogen Peroxide Turbojet-Engine Simulator for Wind-Tunnel Powered-Model Investigations. NACA RM L57H15, 1957.

7. Whitcomb, Richard T.: Recent Results Pertaining to the Application of the "Area Rule." NACA RM L53I15a, 1953.

8. Holdaway George H.: An Experimental Investigation of Reduction in Transonic Drag Rise at Zero Lift by the Addition of Volume to the Fuselage of a Wing-Body-Tail Configuration and a Comparison With Theory. NACA RM A54F22, 1954.

9. Henry, Beverly Z., Jr., and Cahn, Maurice S.: Pressure Distributions Over a Series of Related Afterbody Shapes As Affected by a Propulsive Jet at Transonic Speeds. NACA RM L56K05, 1957.

10. Henry, Beverly Z., Jr., and Cahn, Maurice S.: Additional Results of an Investigation at Transonic Speeds to Determine the Effects of a Heated Propulsive Jet on the Drag Characteristics of a Series of Related Afterbodies. NACA RM L56G12, 1956.

11. McDevitt, John B., and Haire, William M.: Investigation at High Subsonic Speeds of a Body-Contouring Method for Alleviating the Adverse Interference at the Root of a Sweptback Wing. NACA TN 3672, 1956. (Supersedes NACA RM A54A22.)

12. Howell, Robert R., and Braslow, Albert L.: An Experimental Study of a Method of Designing the Sweptback-Wing—Fuselage Juncture for Reducing the Drag at Transonic Speeds. NACA RM L54L31a, 1955.

13. Palmer, William E., Howell, Robert R., and Braslow, Albert L.: Transonic Investigation at Lifting Conditions of Streamline Contouring in the Sweptback-Wing—Fuselage Juncture in Combination With the Transonic Area Rule. NACA RM L56D11a, 1956.

14. Norton, Harry T., Jr., and Swihart, John M.: Effect of a Hot-Jet Exhaust on Pressure Distributions and External Drag of Several Afterbodies on a Single-Engine Airplane Model at Transonic Speeds. NACA RM L57J04, 1957.

TABLE I

COORDINATES OF PRESSURE ORIFICES ON BASIC CONFIGURATION

Orifice Row	Orifice Number	Model station	-y	z	x/d_e	Pressure instrumentation*
Shroud						
ϕ = 180°	1	69.52	2.94	-2.91	-2.37	m
	2	73.27	2.94	-2.50	-1.43	m
	3	75.15	2.94	-2.49	-.96	m
	4	77.02	2.94	-2.30	-.50	m
	5	77.65	2.94	-2.20	-.34	m
	6	78.27	2.94	-2.10	-.18	t
ϕ = 255°	1	73.27	5.35	-0.65	-1.43	m
	2	75.15	5.31	-.65	-.96	m
	3	77.02	5.14	-.60	-.50	m
	4	77.65	5.06	-.57	-.34	m
	5	78.27	4.97	-.54	-.18	t
ϕ = 330°	1	73.27	4.20	2.18	-1.43	m
	2	75.15	4.18	2.16	-.96	m
	3	77.02	4.09	1.99	-.50	m
	4	77.65	4.05	1.90	-.34	m
	5	78.27	4.00	1.82	-.18	t
Base						
ϕ = 30°	1	77.90	1.99	1.66	-0.28	t
ϕ = 90°	2	77.90	1.02	0	-.28	t
ϕ = 120°	3	77.90	1.28	-.95	-.28	t
ϕ = 180°	4	77.90	2.94	-1.92	-.28	t
ϕ = 255°	5	77.90	4.79	-.50	-.28	t
ϕ = 330°	6	77.90	3.90	1.66	-.28	t
Afterbody						
Shoulder	1	69.52	3.74	2.66	-2.37	m
	2	72.52	3.57	2.60	-1.62	m
	3	73.27	3.36	2.74	-1.43	m
	4	75.15	3.07	2.78	-.96	m
	5	77.02	2.84	2.88	-.50	m
	6	78.27	2.68	2.94	-.18	m
	7	78.90	2.62	2.97	-.03	m
	8	79.52	2.54	3.00	.13	m
	9	80.15	2.47	3.05	.29	m
	10	81.40	2.32	3.11	.60	m
	11	83.90	2.05	3.31	1.23	m
	12	86.39	1.76	3.50	1.85	m

Orifice Row	Orifice Number	Model station	-y	z	x/d_e	Pressure instrumentation*
Afterbody						
ϕ = 30°	1	73.27	1.62	2.19	-1.43	t
	2	78.27	1.73	2.02	-.18	t
	3	78.90	1.85	1.87	-.03	t
	4	79.52	1.80	1.90	.13	t
	5	80.15	1.75	1.99	.29	t
	6	81.40	1.64	2.17	.60	t
	7	82.65	1.54	2.36	.91	t
	8	83.90	1.43	2.55	1.23	t
	9	86.39	1.25	2.93	1.85	t
	10	88.92	1.03	3.14	2.48	t
	11	91.40	.86	3.56	3.10	t
	12	93.91	.66	3.86	3.73	t
	13	96.41	.48	4.18	4.35	t
	14	98.90	.28	4.53	4.98	t
ϕ = 60°	1	78.90	1.02	1.01	-0.03	t
	2	79.52	.98	1.02	.13	m
	3	81.40	.74	1.19	.60	m
	4	83.90	.40	1.31	1.23	m
	5	86.39	.09	1.57	1.85	t
ϕ = 90°	1	78.90	0.72	-0.06	-0.03	t
	2	79.52	.71	-.08	.13	t
	3	80.15	.64	-.07	.29	t
	4	81.40	.48	-.08	.60	t
	5	82.65	.33	-.08	.91	t
Fuselage bottom C_L	1	69.52	0	-2.65	-2.37	m
	2	72.52	0	-2.35	-1.62	m
	3	77.02	0	-1.76	-.50	m
	4	78.27	.01	-1.55	-.18	t
	5	78.90	-.01	-1.43	-.03	t
	6	79.52	0	-1.32	.13	t
	7	80.15	-.01	-1.19	.29	t
	8	81.40	-.01	-.93	.60	t
	9	83.90	-.01	-.28	1.23	t
	10	88.92	0	2.48	2.48	t
	11	99.62	-.01	4.70	5.16	m
	12	100.45	-.05	6.14	5.36	m

*t = transducer; m = manometer.

TABLE II

COORDINATES OF PRESSURE ORIFICES ON MODIFIED CONFIGURATION

Orifice		Model station	-y	z	x/d_e	Pressure instrumentation*
Row	Number					
Fairings						
Fuselage bottom C_L	1	58.73	0.24	-4.24	-5.07	m
	2	62.97	.26	-4.33	-4.01	m
	3	67.17	.27	-4.02	-2.96	m
	4	71.18	.27	-3.24	-1.96	m
	5	73.18	.28	-2.74	-1.46	m
	6	75.11	.28	-2.21	-.97	t
	7	77.04	0	-1.76	-.49	m
	8	78.28	.01	-1.55	-.18	t
	9	78.89	-.01	-1.43	-.03	t
$\phi \approx 180°$	1	59.27	3.08	-4.04	-4.93	m
	2	63.31	3.12	-4.01	-3.92	m
	3	67.34	3.13	-3.70	-2.91	m
	4	71.36	3.12	-3.21	-1.91	m
	5	74.43	3.06	-2.79	-1.14	m
	6	76.43	3.02	-2.51	-.64	m
	7	78.44	3.02	-2.17	-.14	m
$\phi \approx 235°$	1	59.37	6.33	-2.42	-4.91	m
	2	63.36	6.37	-2.37	-3.91	m
	3	67.50	6.20	-2.15	-2.87	t
	4	71.51	5.83	-1.78	-1.87	t
	5	74.45	5.43	-1.47	-1.14	t
	6	76.44	5.11	-1.27	-.64	t
	7	78.43	4.85	-1.01	-.14	t
$\phi \approx 320°$	1	58.73	5.20	3.03	-5.07	m
	2	62.74	5.34	3.00	-4.08	m
	3	65.74	5.32	2.92	-3.31	m
	4	68.75	5.23	2.75	-2.56	t
	5	70.66	5.11	2.62	-2.09	m
	6	72.63	4.93	2.45	-1.59	t
	7	74.63	4.72	2.24	-1.09	t
	8	76.57	4.50	1.95	-.61	t
	9	78.27	4.00	1.82	-.18	t
Base						
$\phi = 30°$ $\phi = 90°$ $\phi = 120°$ $\phi = 180°$ $\phi = 255°$ $\phi = 330°$	1 2 3 4 5 6	77.90 77.90 77.90 77.90 77.90 77.90	1.99 1.02 1.28 2.94 4.79 3.90	1.66 0 -.95 -1.92 -.50 1.66	-0.28 -.28 -.28 -.28 -.28 -.28	t t t t t t

*t = transducer; m = manometer.

Orifice		Model station	-y	z	x/d_e	Pressure instrumentation*
Row	Number					
Afterbody						
Shoulder	1	77.02	2.84	2.88	-0.50	m
	2	78.27	2.68	2.94	-.18	m
	3	78.90	2.62	2.97	-.03	m
	4	79.52	2.54	3.00	.13	m
	5	80.15	2.47	3.05	.29	m
	6	81.40	2.32	3.11	.60	m
	7	83.90	2.05	3.31	1.23	m
	8	86.39	1.76	3.50	1.85	m
$\phi = 30°$	1	78.27	1.73	2.02	-0.18	t
	2	78.90	1.85	1.87	-.03	t
	3	79.52	1.80	1.90	.13	t
	4	80.15	1.75	1.99	.29	t
	5	81.40	1.64	2.17	.60	t
	6	82.65	1.54	2.36	.91	t
	7	83.90	1.43	2.55	1.23	t
	8	86.39	1.25	2.93	1.85	t
	9	91.40	.86	3.56	3.10	t
	10	96.41	.48	4.18	4.35	t
$\phi = 60°$	1	78.90	1.02	1.01	-0.03	t
	2	79.52	.98	1.02	.13	m
	3	81.40	.74	1.19	.60	m
	4	83.90	.40	1.31	1.23	m
	5	86.39	.09	1.57	1.85	t
$\phi = 90°$	1	78.90	0.72	-0.06	-0.03	t
	2	79.52	.71	-.08	.13	t
	3	81.40	.48	-.08	.60	t
	4	82.65	.33	-.08	.91	t
Fuselage bottom C_L	1	79.52	0	-1.32	0.13	t
	2	80.15	-.01	-1.19	.29	t
	3	81.40	-.01	-.93	.60	t
	4	83.90	-.01	-.28	1.23	t
	5	99.62	-.01	4.70	5.16	m
	6	100.45	-.05	6.14	5.36	m

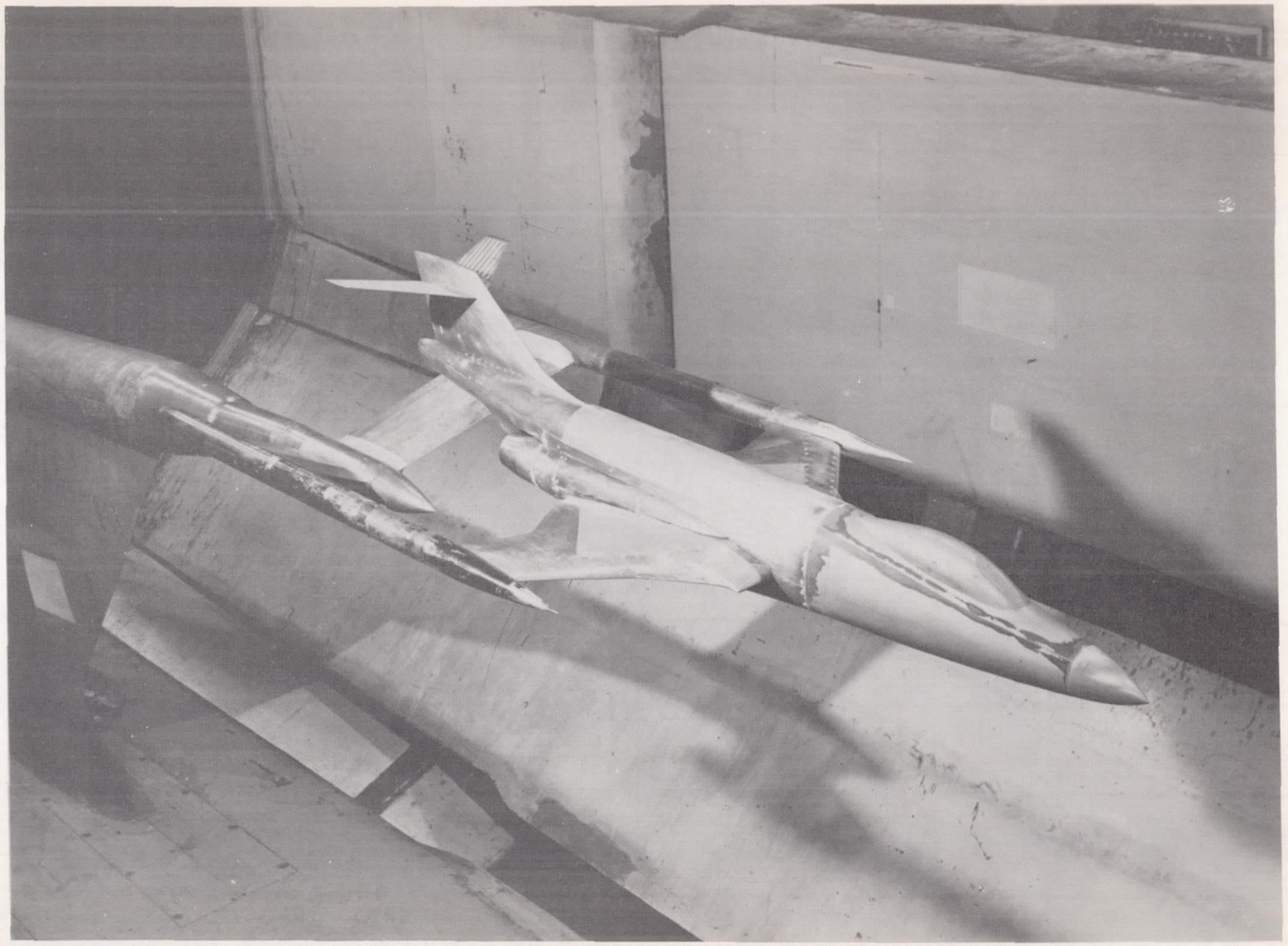

(a) Three-quarter front view. L-95566

Figure 1.- Photograph of basic twin-engine jet-exit model.

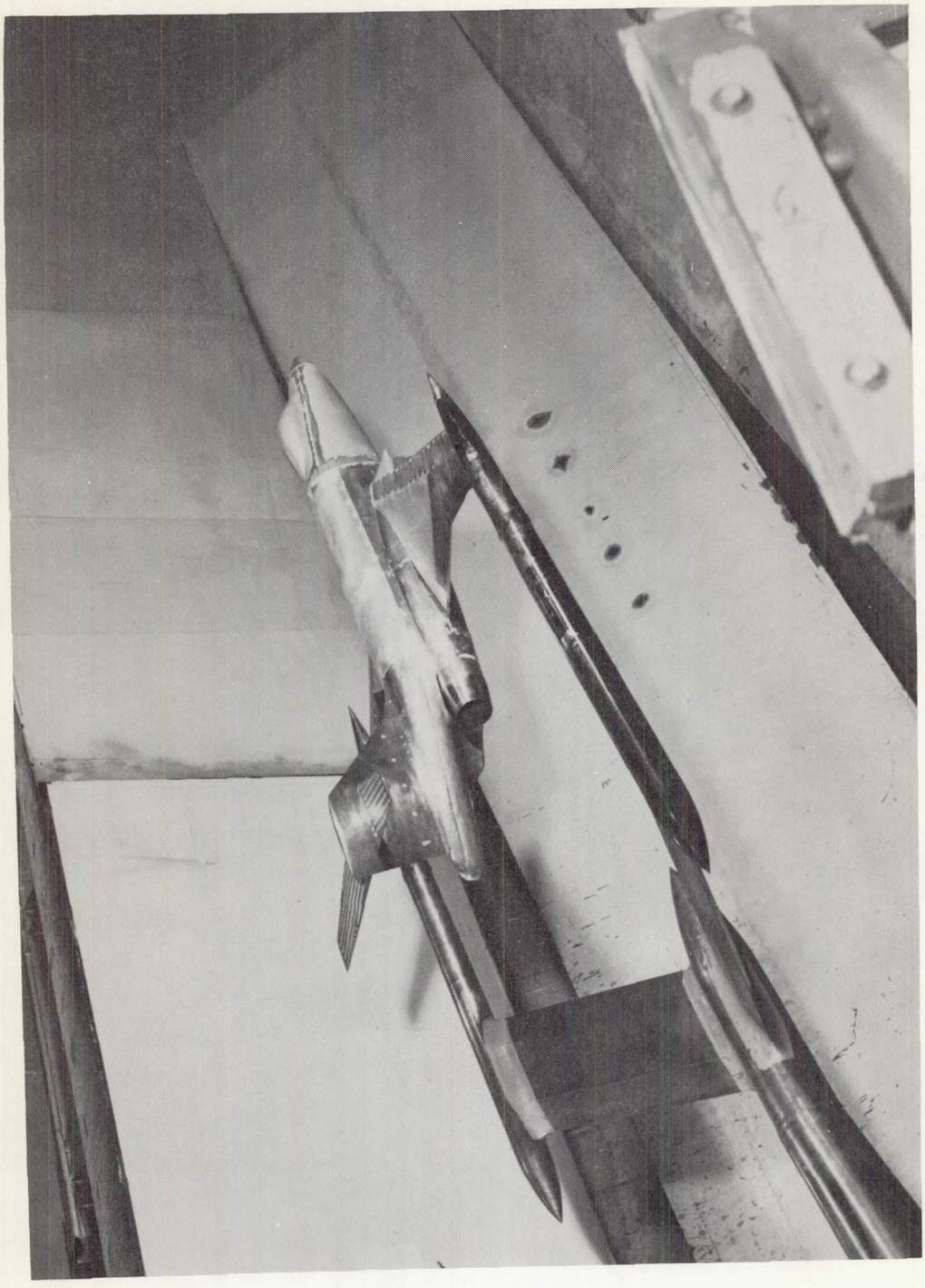

L-95567

(b) Three-quarter rear view.

Figure 1.- Continued.

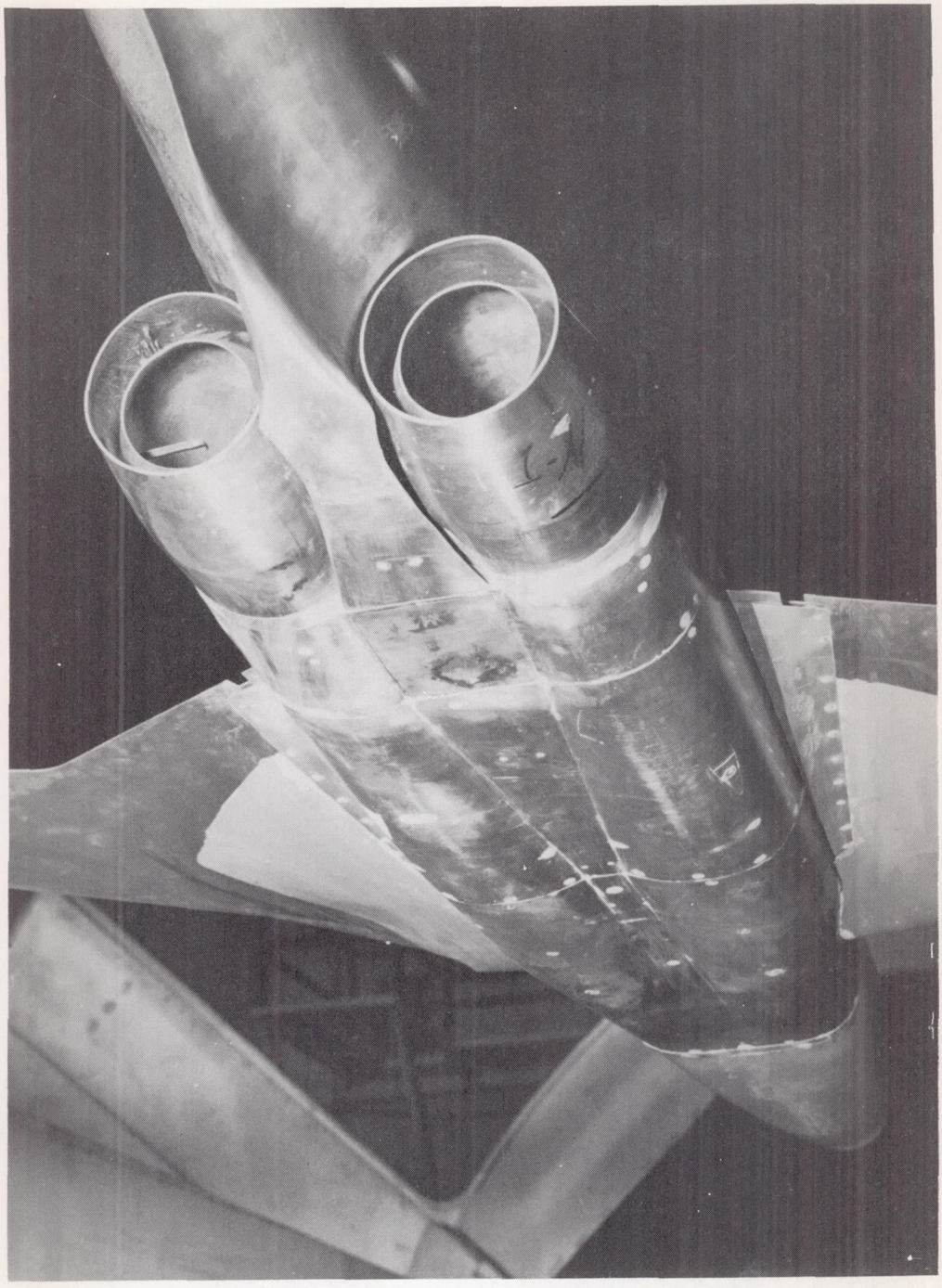

(c) Bottom view of jet exits. L-95565

Figure 1.- Concluded.

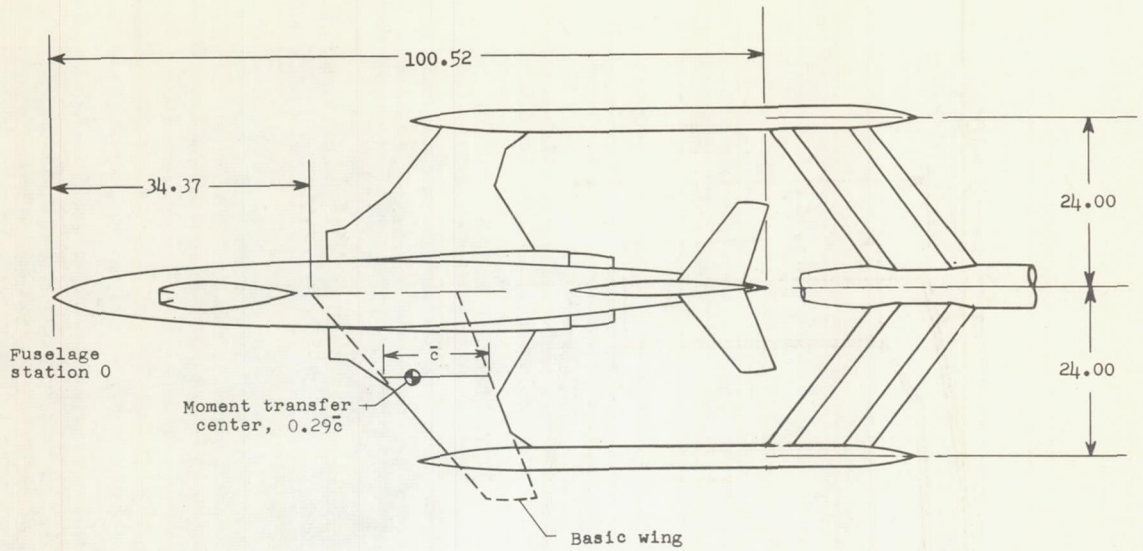

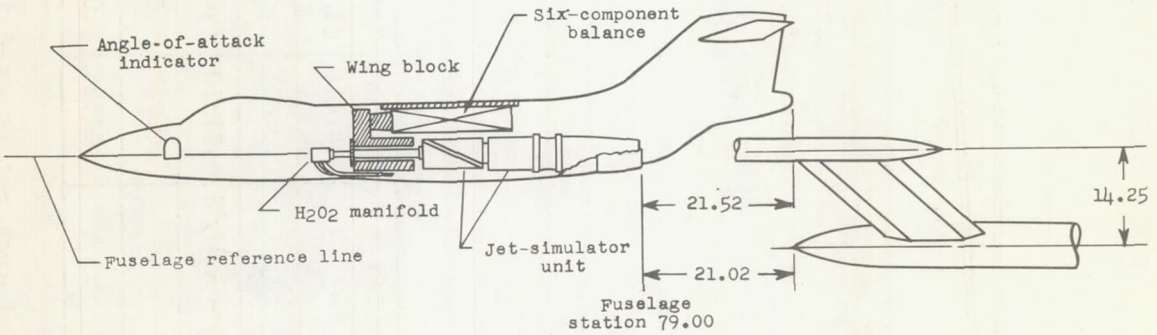

ITEM	WING, BASIC (SHOWN BY DASHED LINES)	HORIZONTAL TAIL	VERTICAL TAIL
Area, sq ft	5.75	1.17	1.18[2]
Span, ft	4.95	1.97	0.94
Aspect ratio	4.28	3.30	
Mean aerodynamic chord, ft	1.28	0.62	1.46[2]
Taper ratio	0.28	0.46	
Incidence angle, deg	1.00	0.00	
Dihedral angle, deg	0.00	10.00	
Sweepback of leading edge, deg	41.12	39.80	52.00
Sweepback of trailing edge, deg	19.42	20.93	16.60
Root airfoil section	NACA 65A007[1]	65A007	65A007
Tip airfoil section	NACA 65A006[1]	65A006	65A007

1 The wing airfoil sections were modified by extending the chord 5 percent forward of the 16.04-percent-chord line and incorporating 1.67 percent positive camber.
2 Basic, excluding dorsal.

Figure 2.- Sketch of basic model and geometric details. All dimensions are in inches unless otherwise noted.

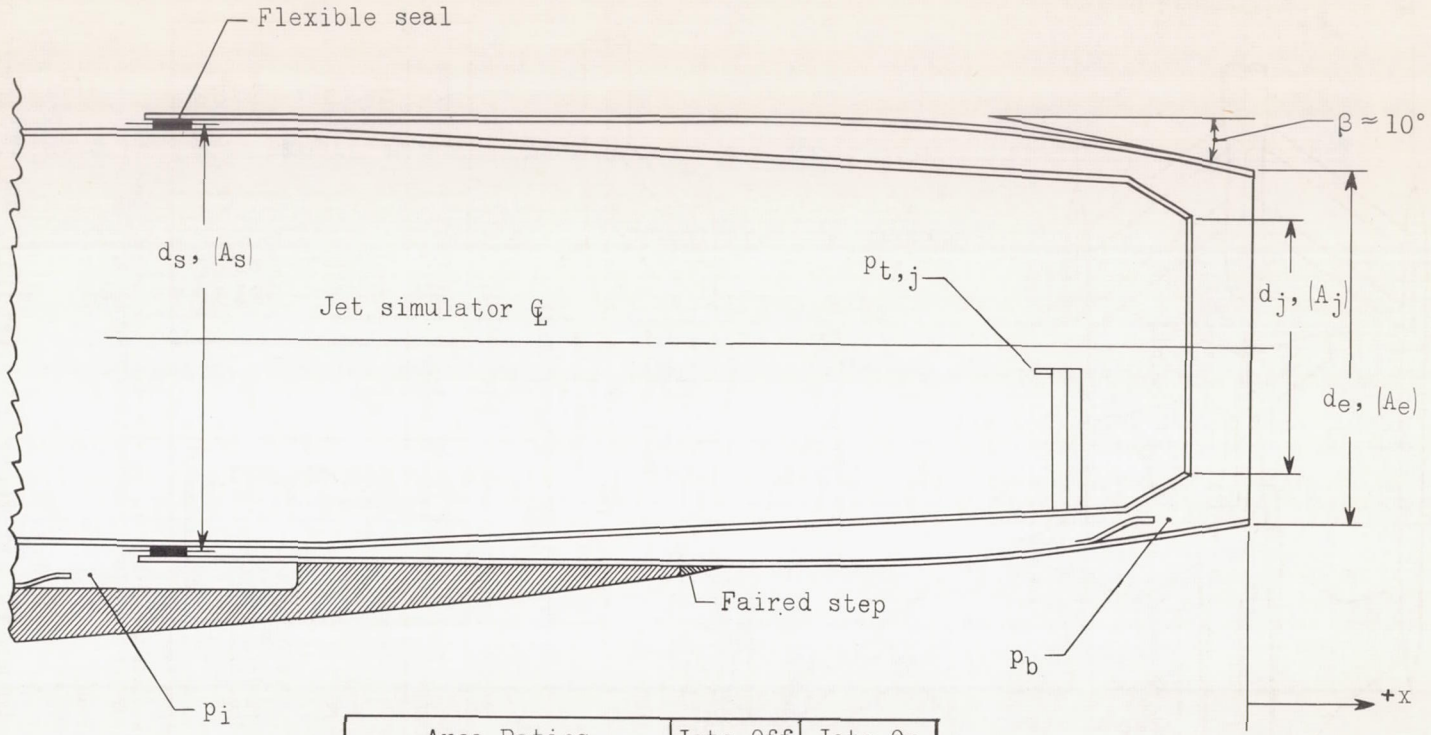

Area Ratios	Jets Off	Jets On
A_j/S	0.01491	0.01522
A_e/S	.03001	.03036
$A_b/S = (A_e - A_j)/S$	.01510	.01514
$(A_s - A_j)/S$	.02933	.02902
A_s/S	.04424	.04424

Figure 3.- Pressure instrumentation and area ratios used in determination of fuselage-tail drag coefficient. Seal and exit areas are given for two engines. S = 5.75 sq ft.

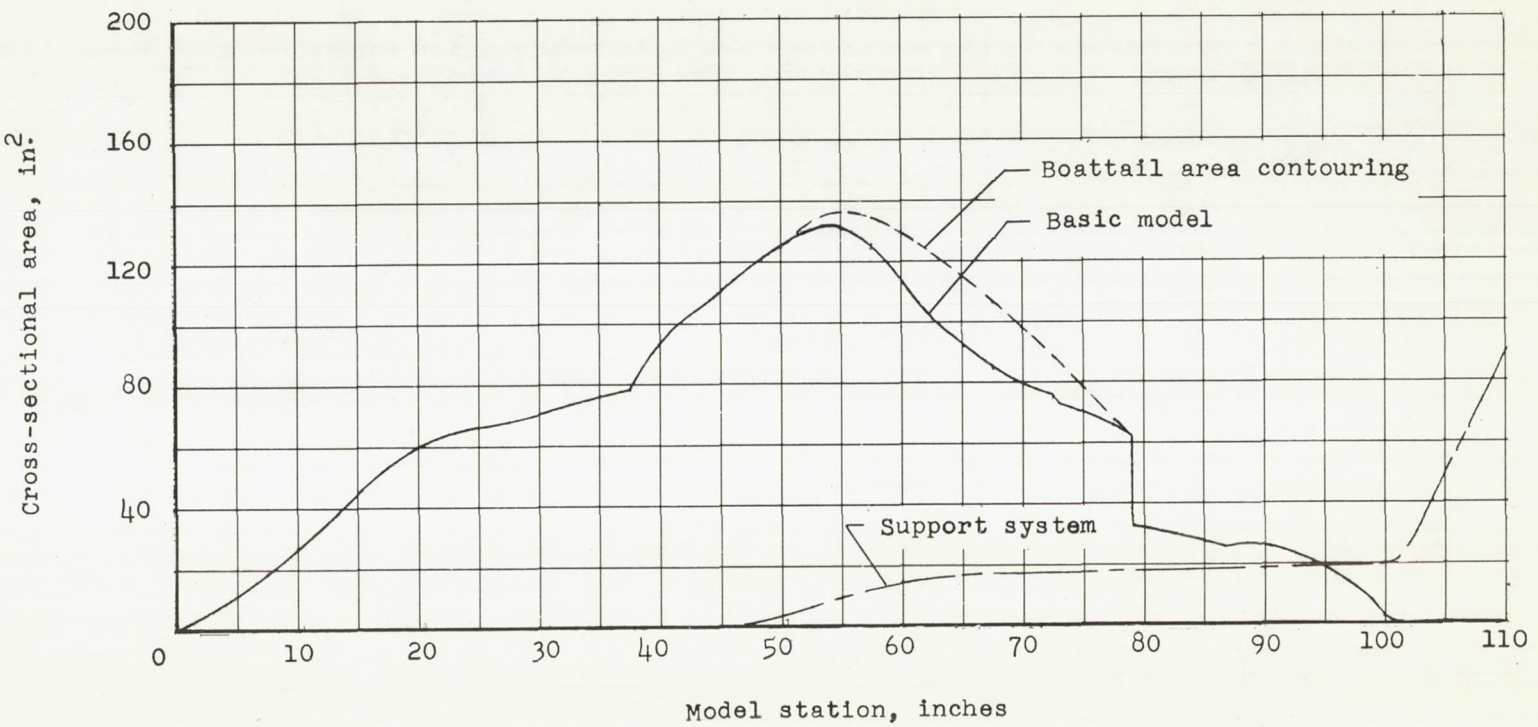

Figure 4.- Area progressions of basic model and model with boattail area contouring.

(a) Fuselage cross sections showing area contouring additions. Fuselage stations measured from model nose.

Figure 5.- Details of boattail area contouring.

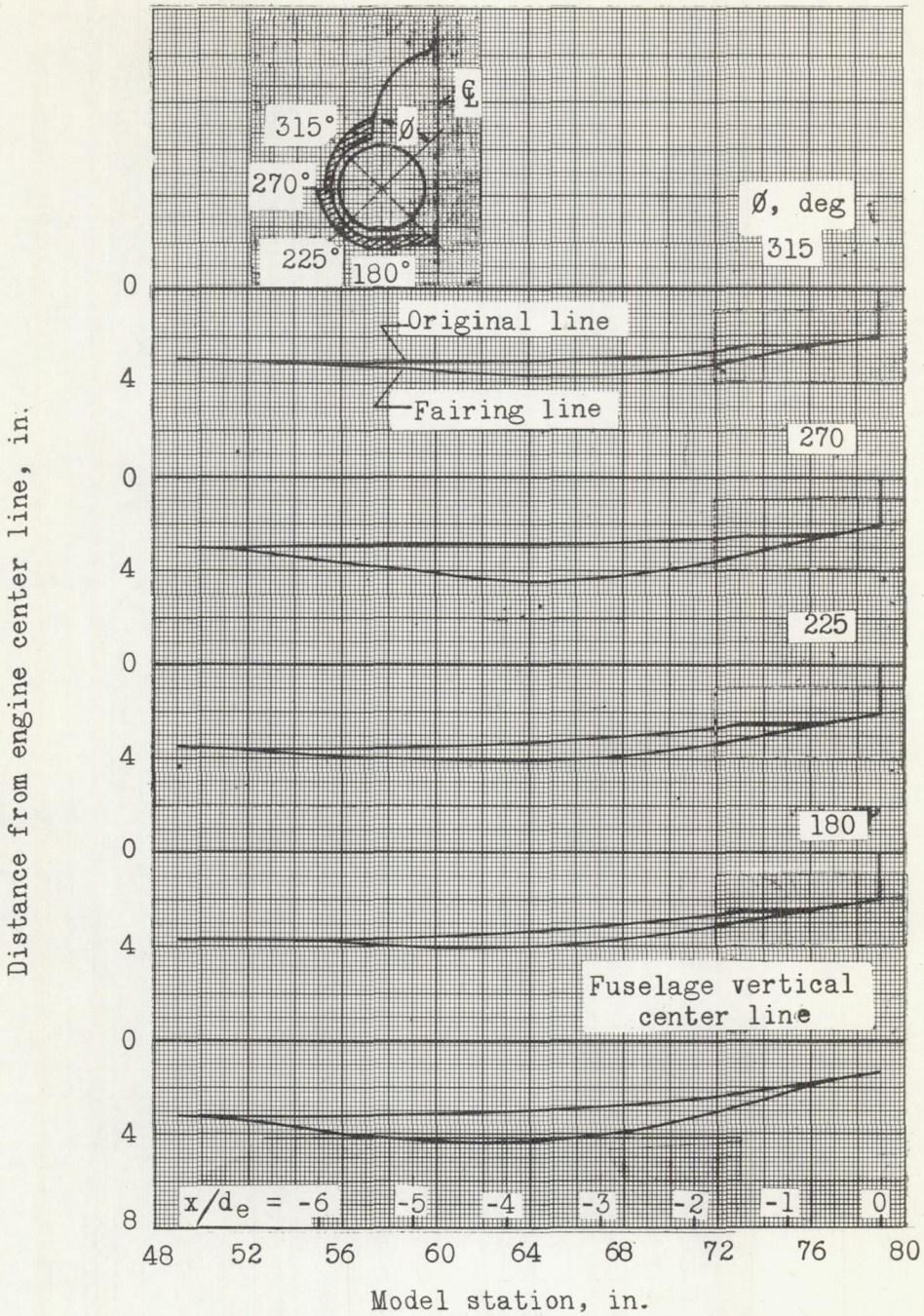

(b) Longitudinal sections of basic model and model with boattail area contouring.

Figure 5.- Concluded.

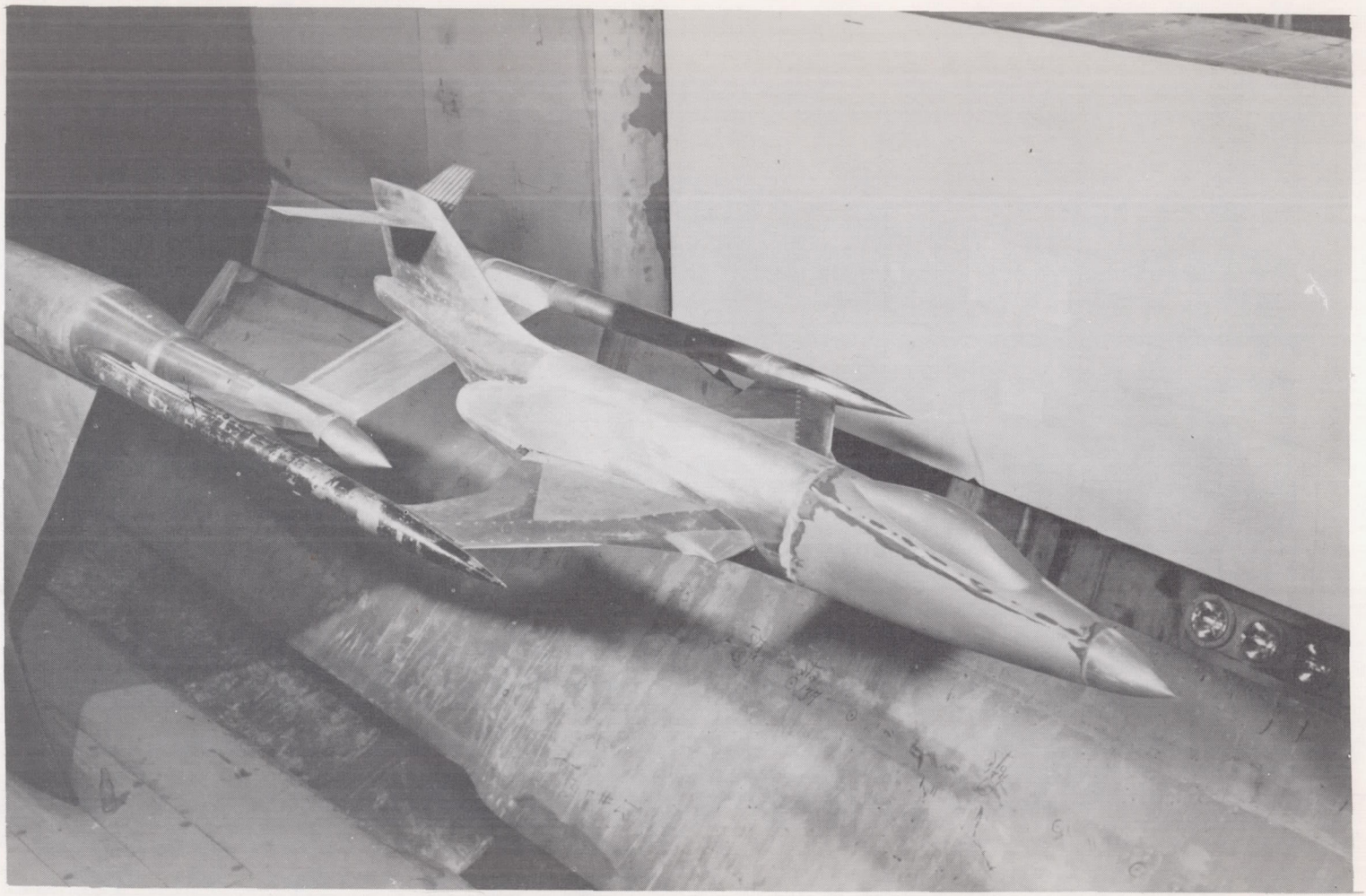

(a) Three-quarter front view. L-94185

Figure 6.- Photographs of model with boattail area contouring.

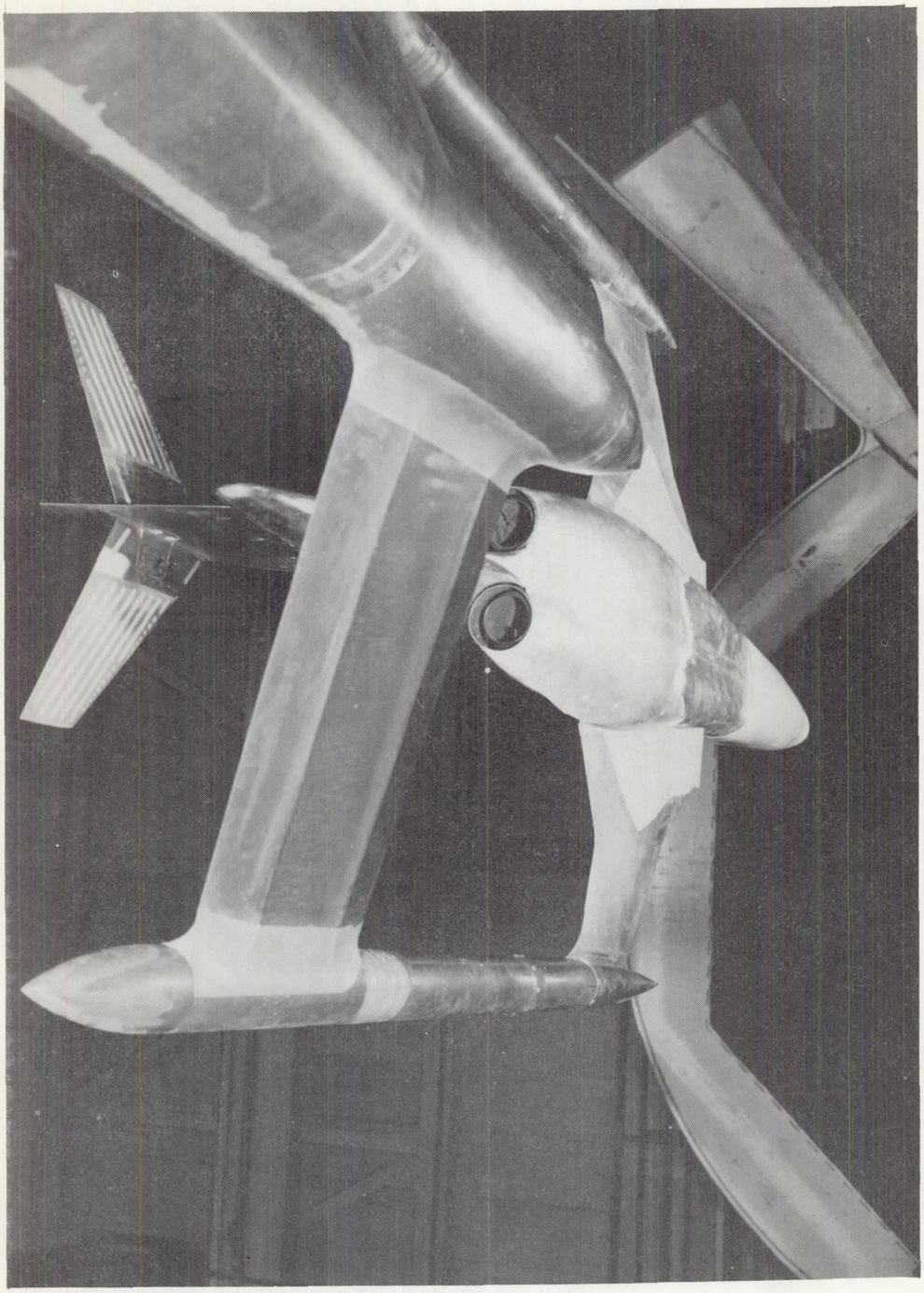

L-94186

(b) Rear underside view.

Figure 6.- Continued.

(c) Close-up view of fairings. L-94187

Figure 6.- Concluded.

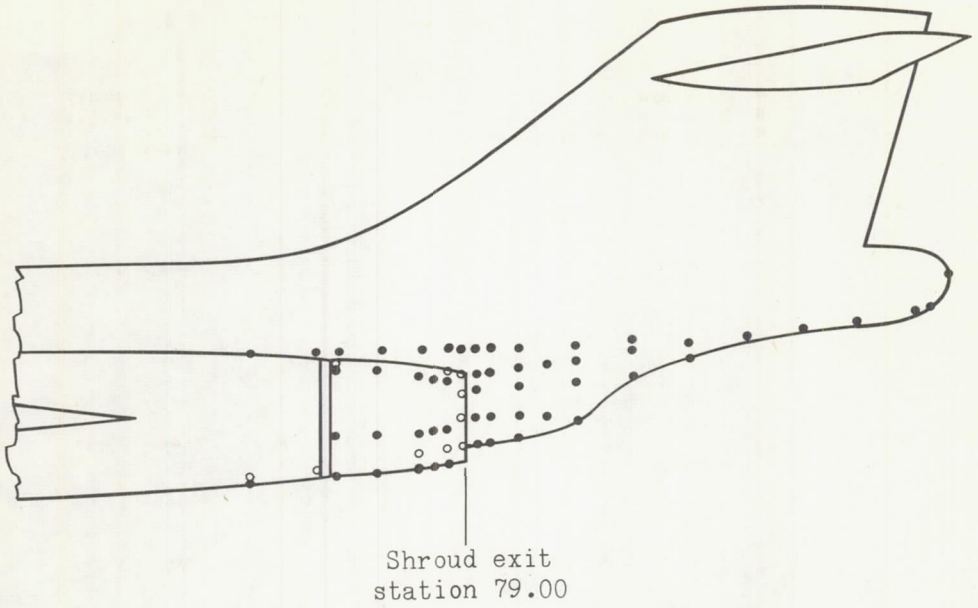

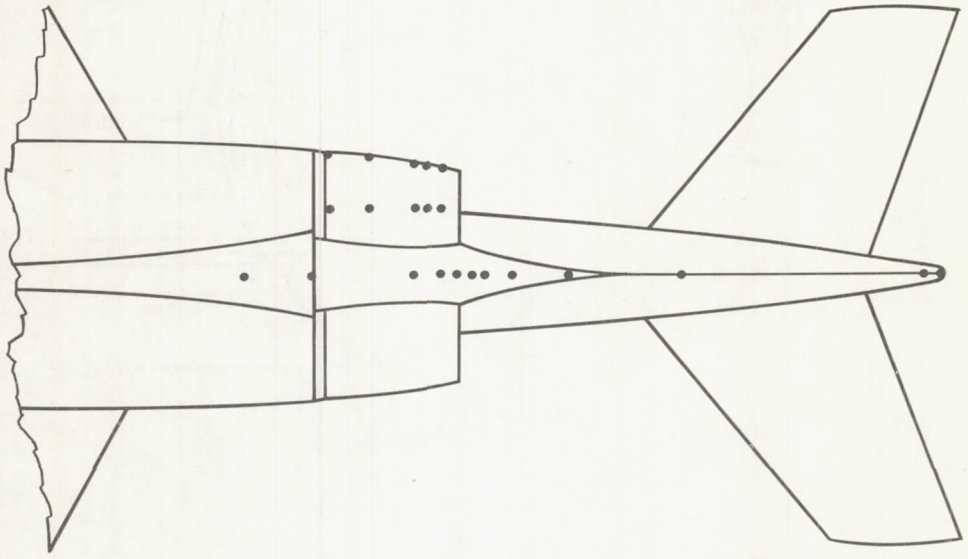

(a) Left side and bottom views.

Figure 7.- General arrangement of external orifices on basic model. See table I for orifice coordinates. Open symbols are orifices which are hidden from view.

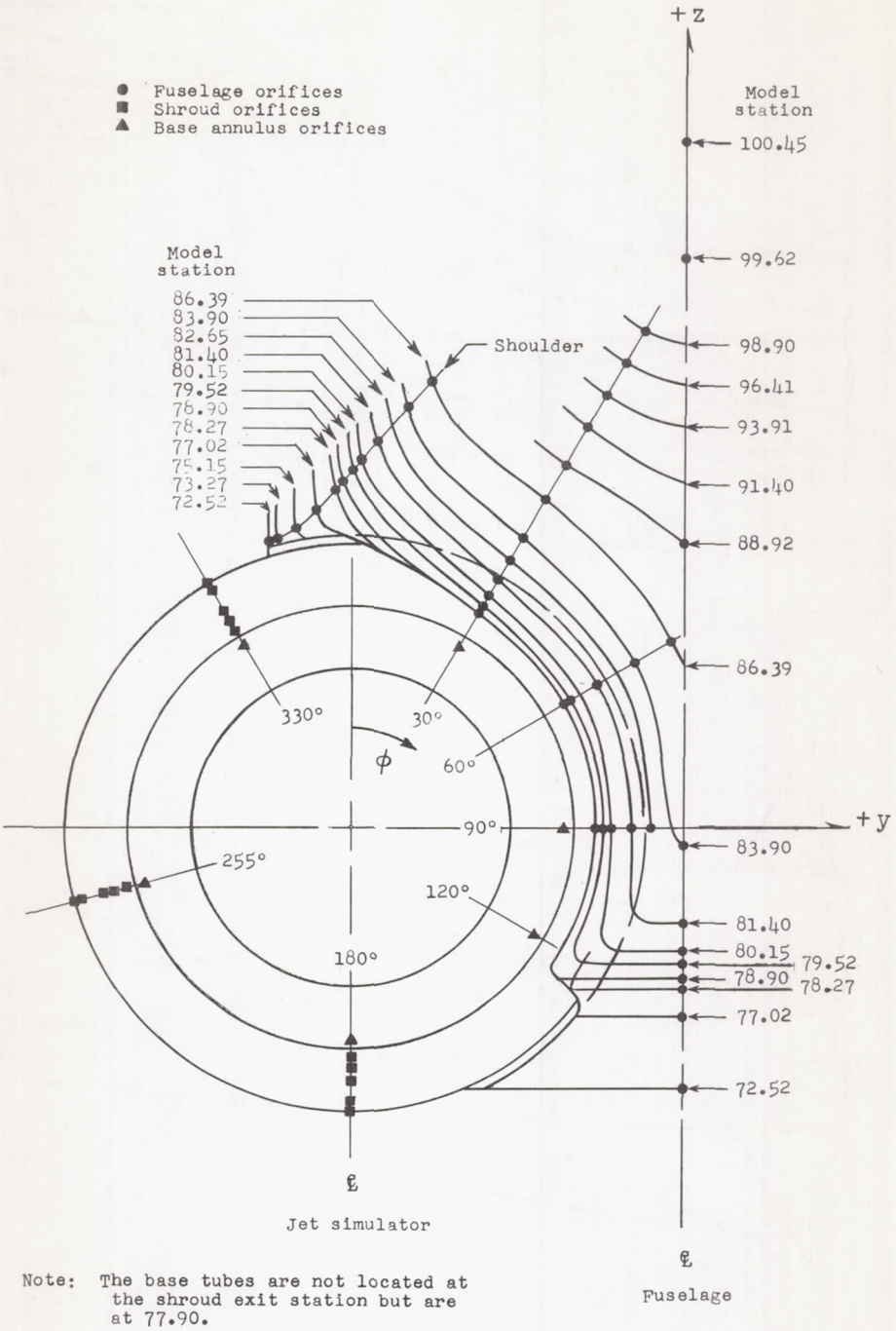

Note: The base tubes are not located at the shroud exit station but are at 77.90.

(b) Rear view of left side.

Figure 7.- Concluded.

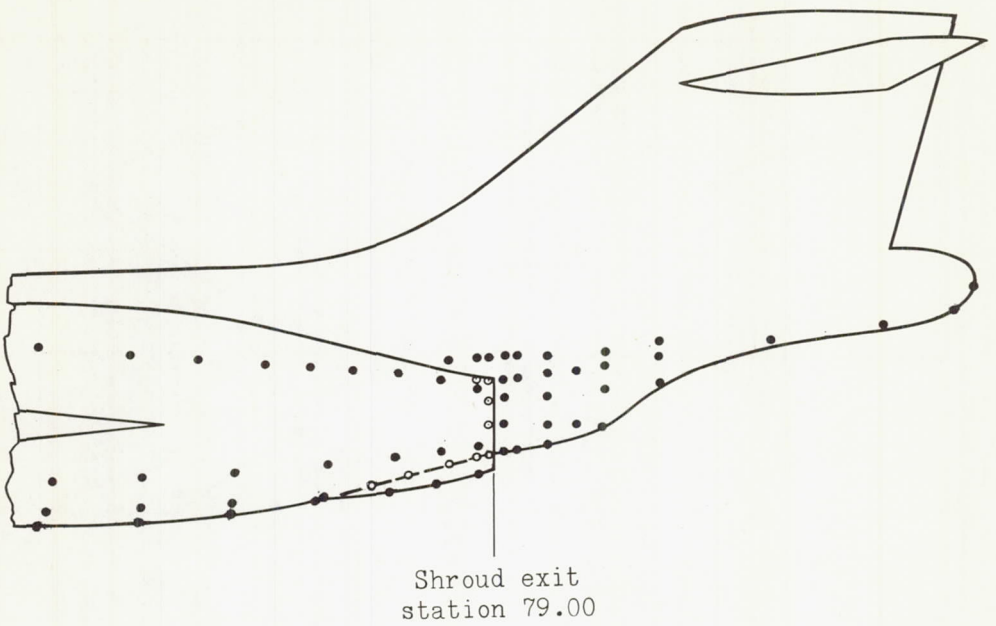

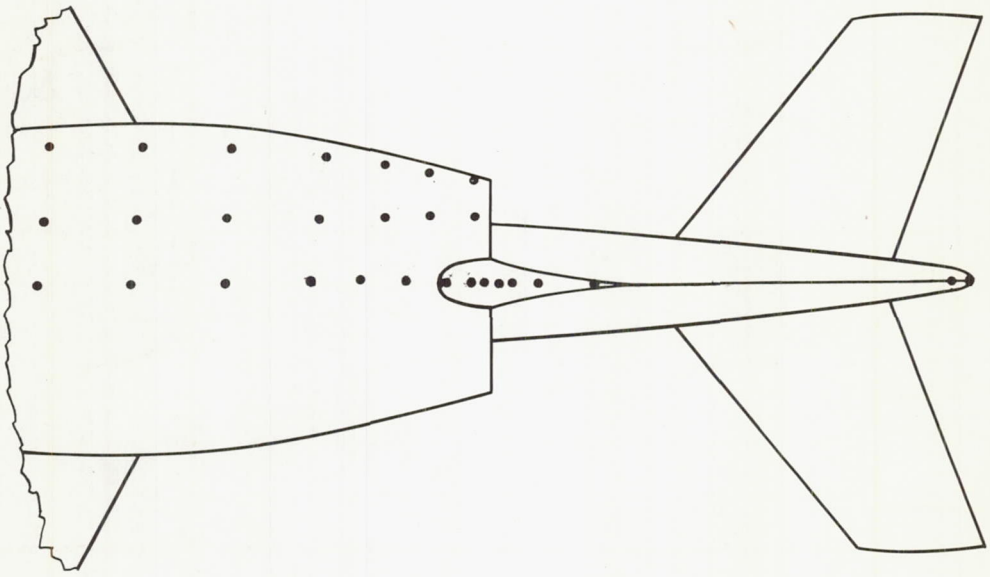

Figure 8.- General arrangement of external orifices on modified model. Left side and bottom views. See table II for orifice coordinates. Open symbols are orifices which are hidden from view.

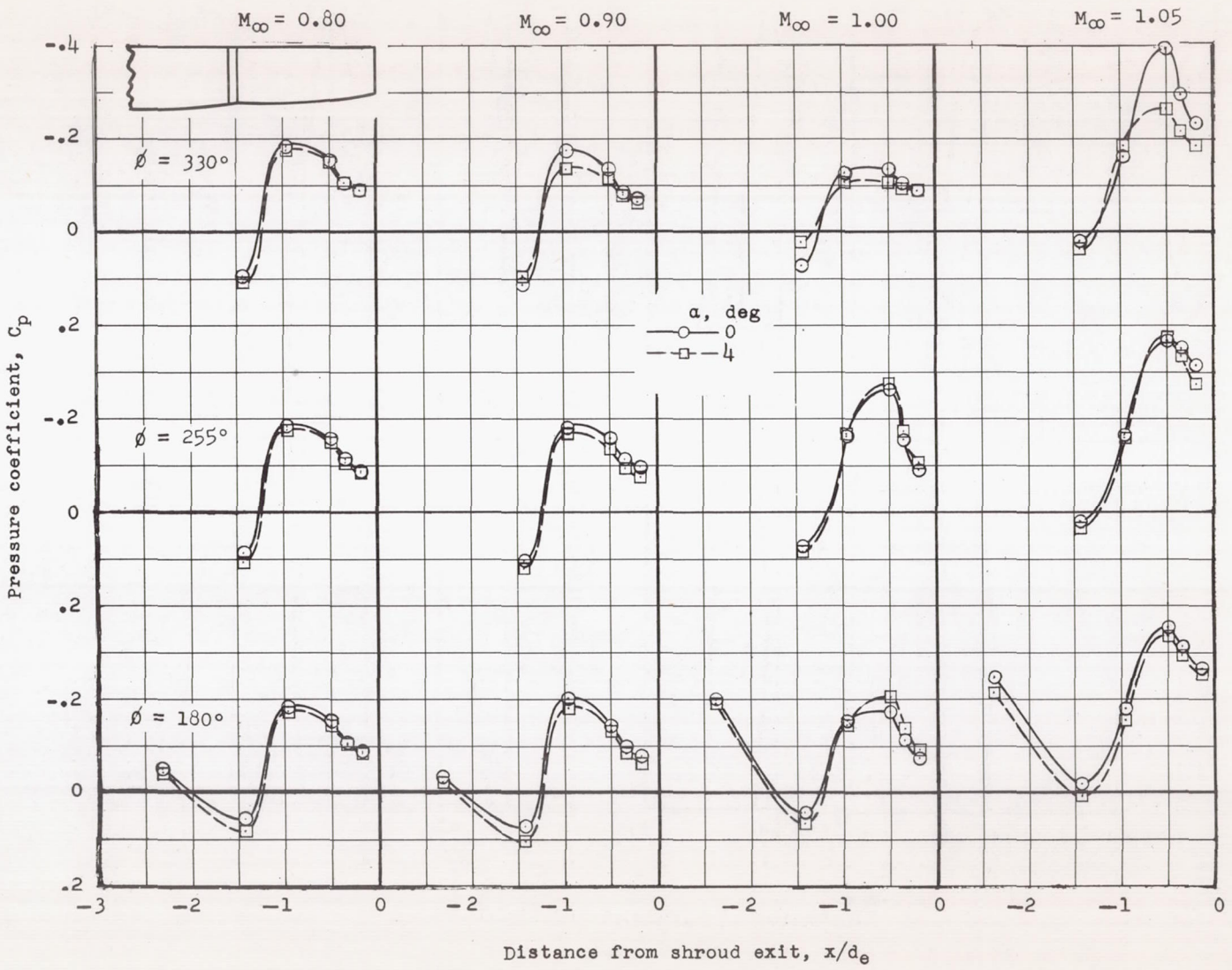

Figure 9.- Pressure distributions on engine shroud of basic model. Jets off.

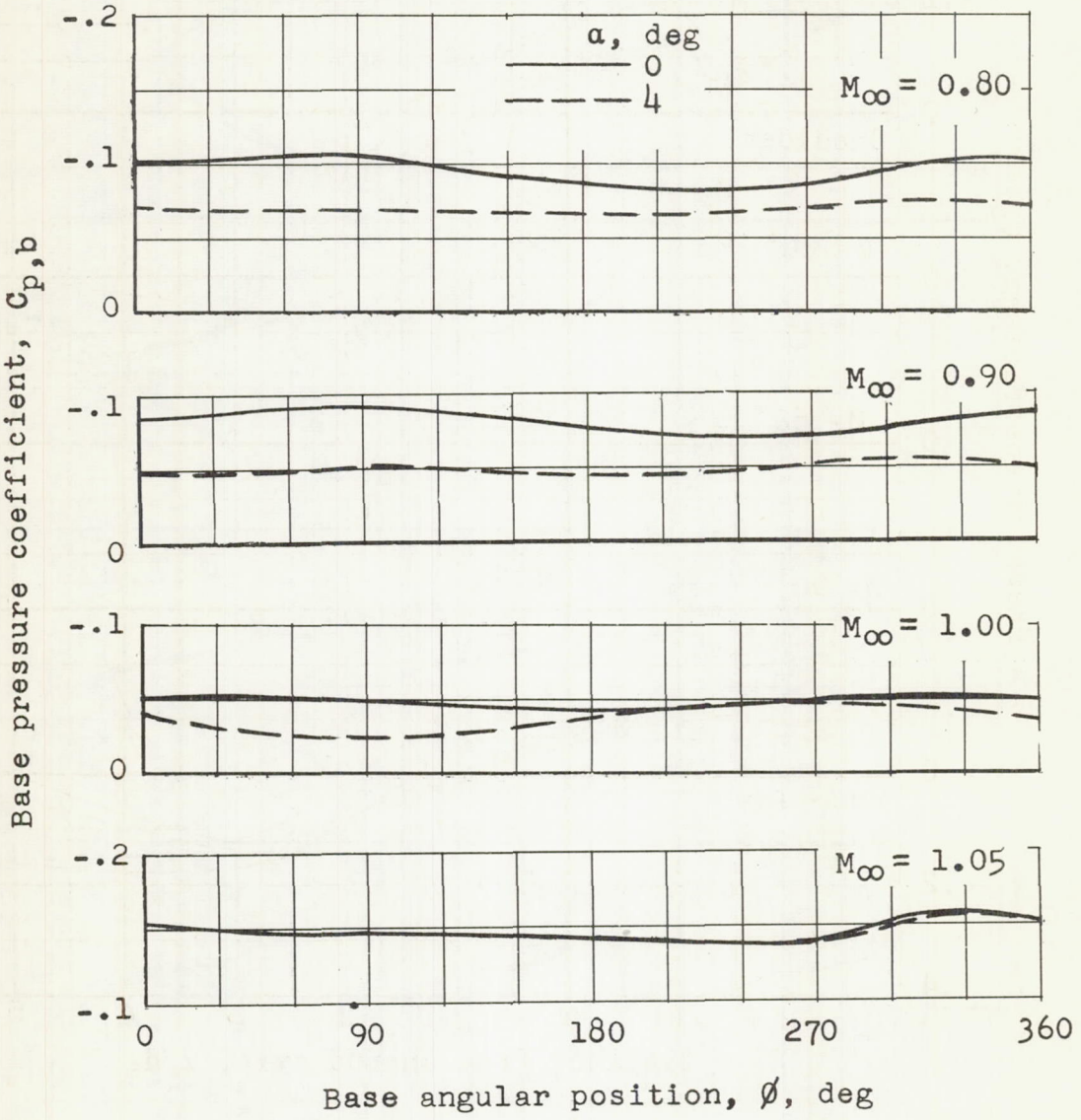

Figure 10.- Angular variation of base pressure coefficient for basic model. Jets off.

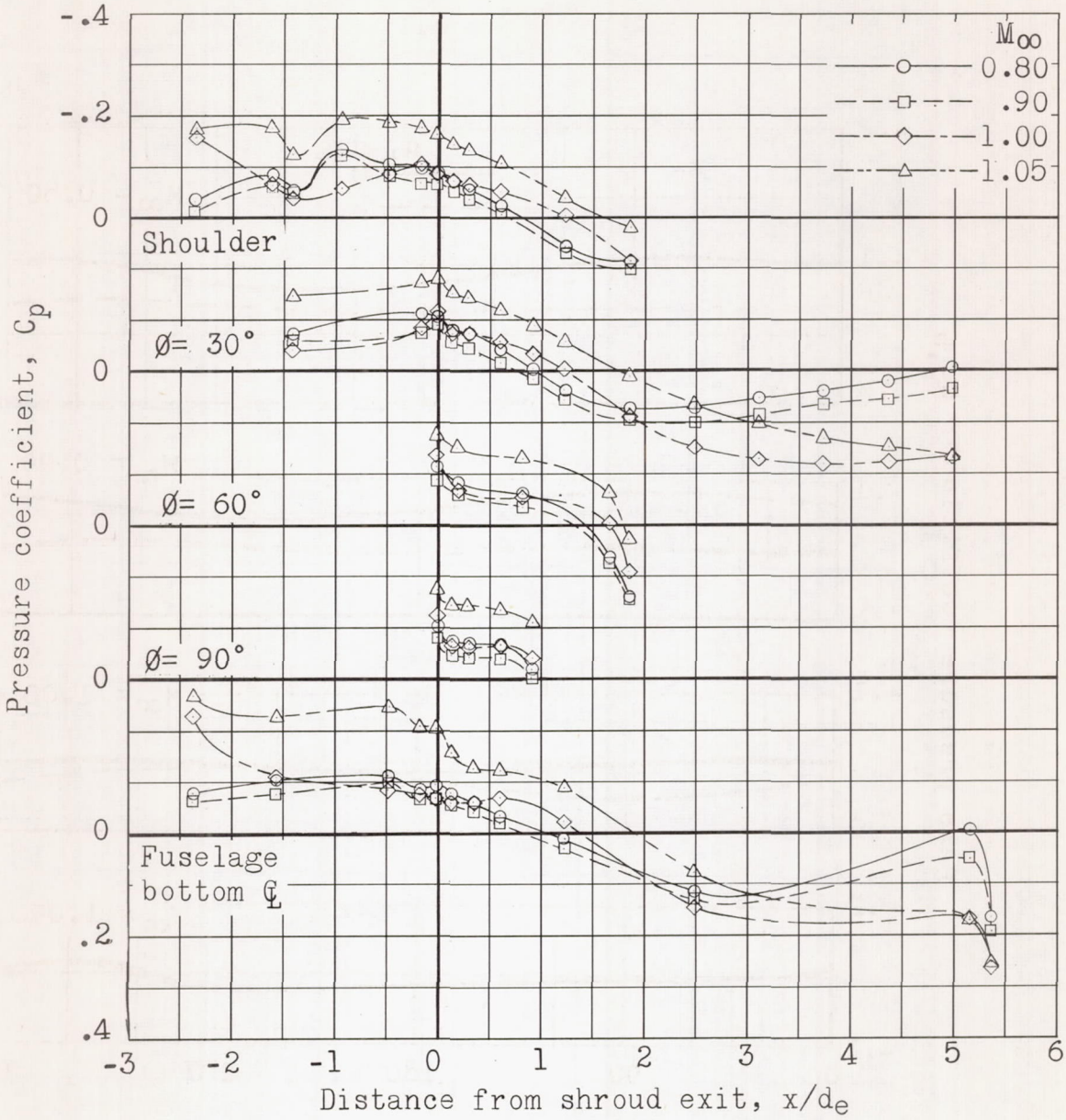

(a) $\alpha = 0^\circ$.

Figure 11.- Pressure distributions along afterbody of basic model. Jets off.

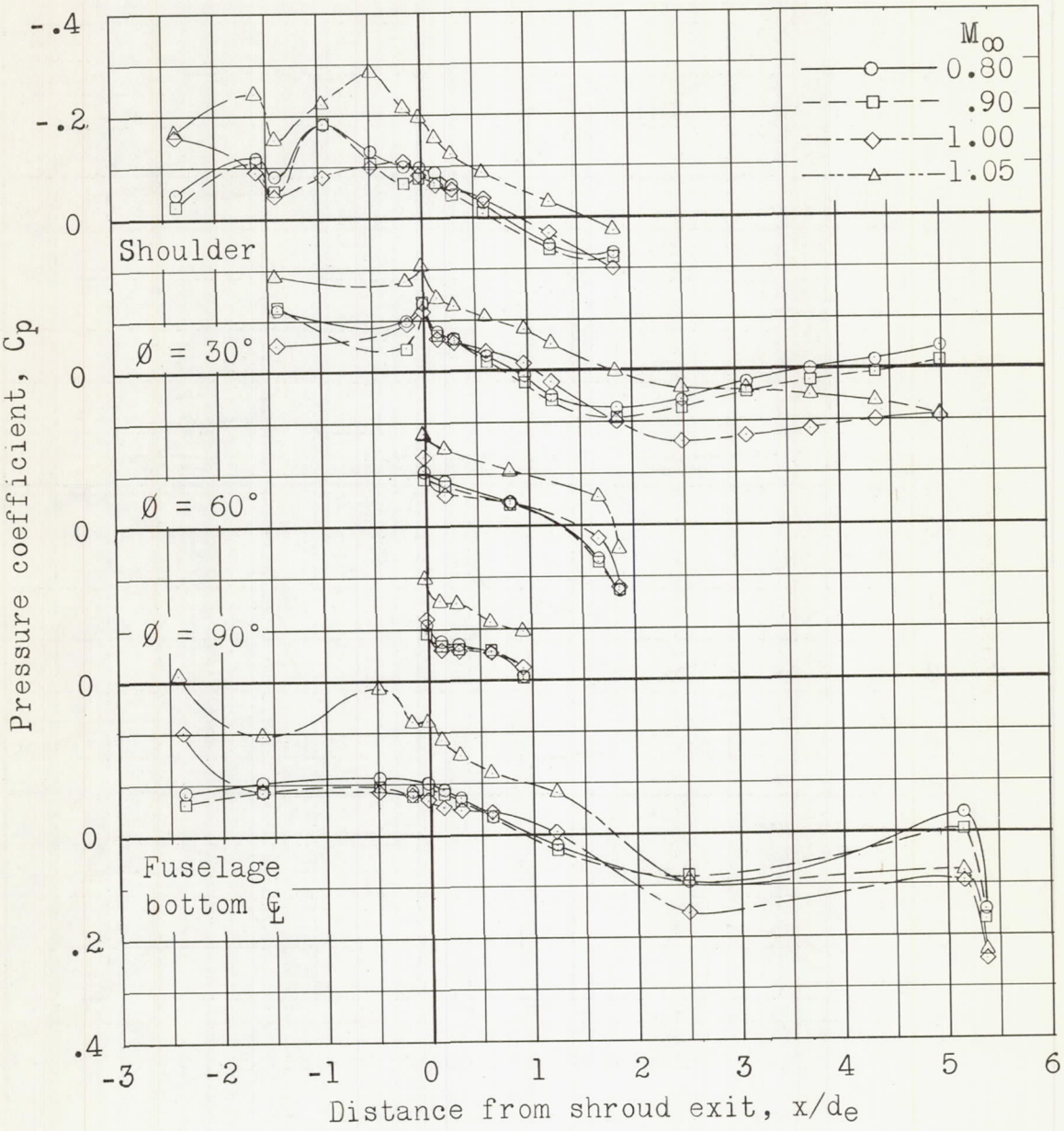

(b) $\alpha = 4^\circ$.

Figure 11.- Concluded.

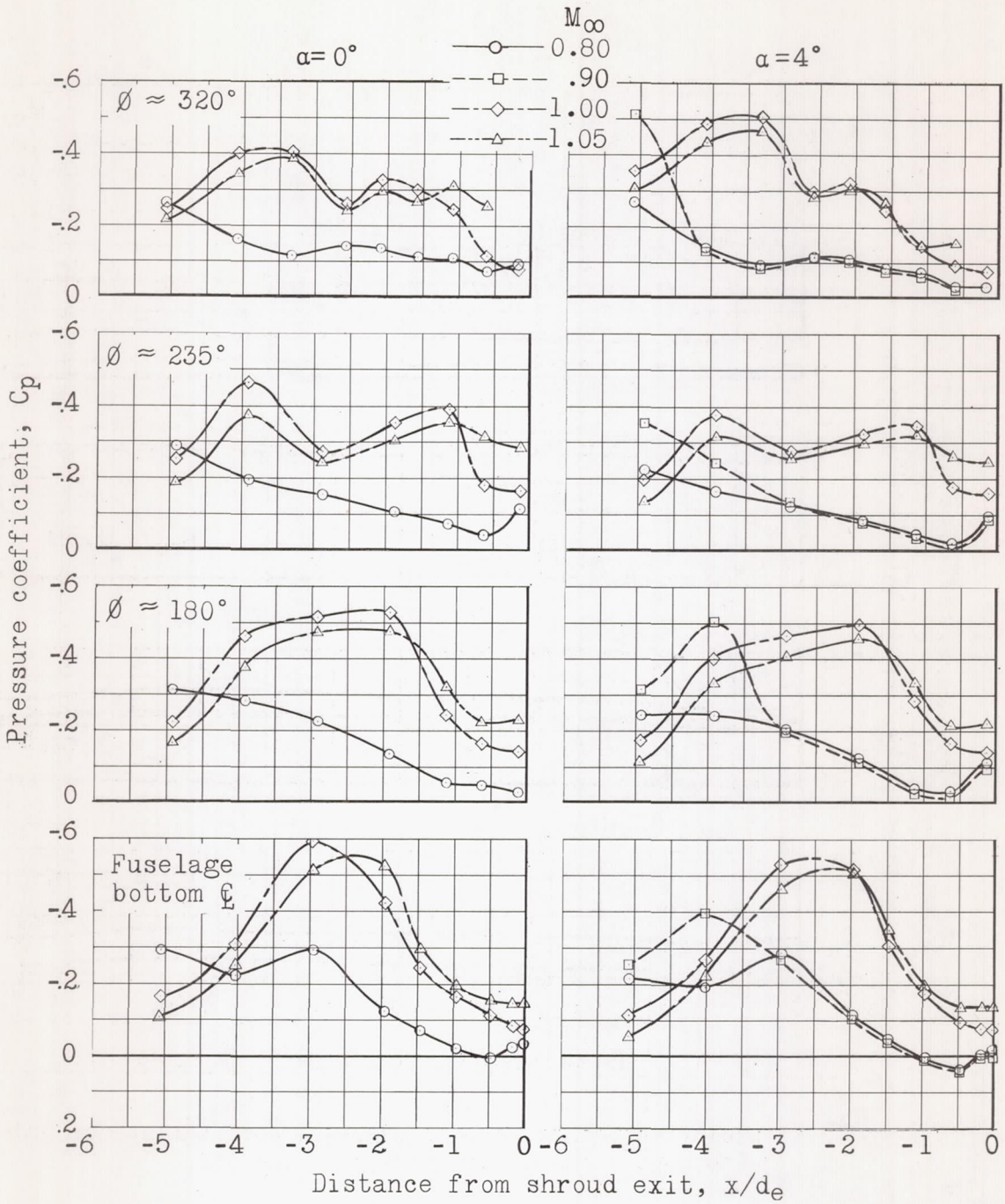

Figure 12.- Pressure distributions along boattail area contouring fairing. Jets off.

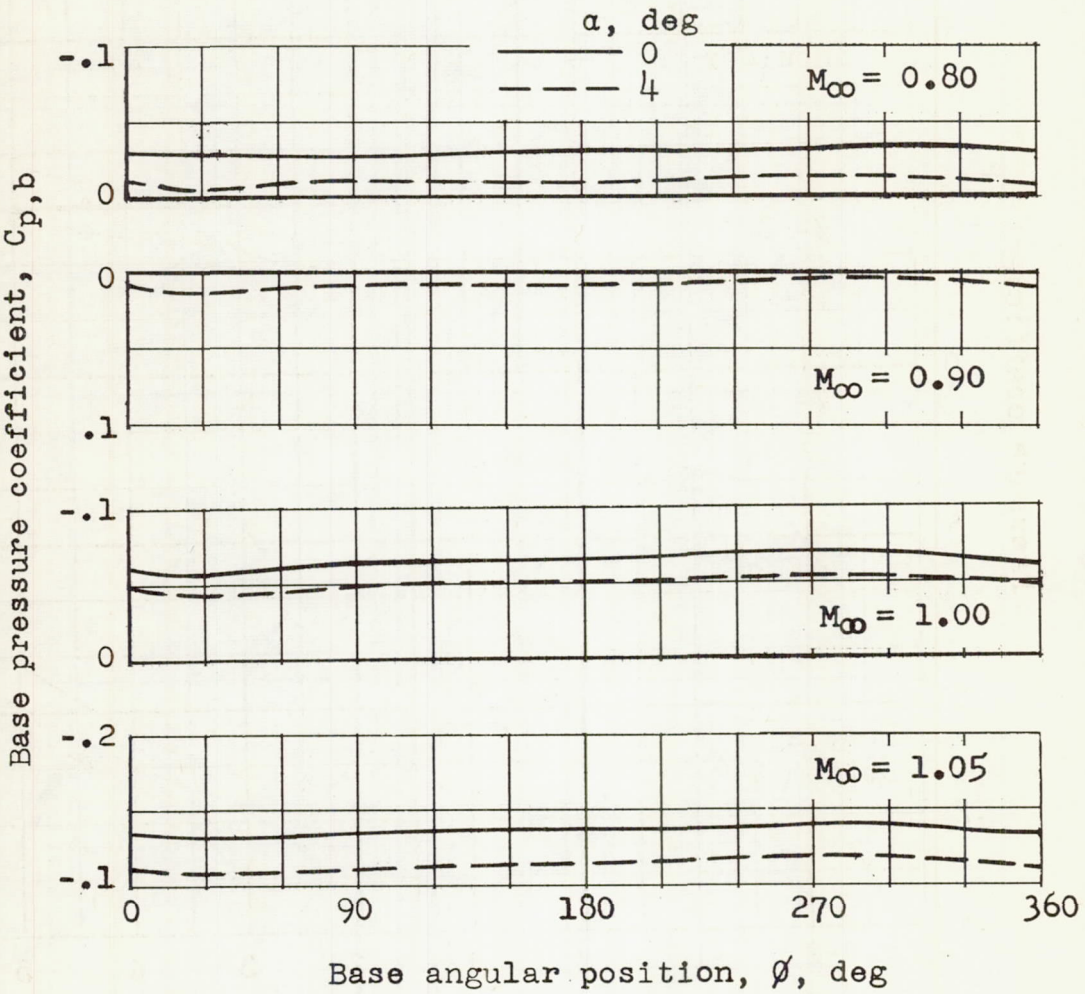

Figure 13.- Angular variation of base pressure coefficient for model with boattail area contouring. Jets off.

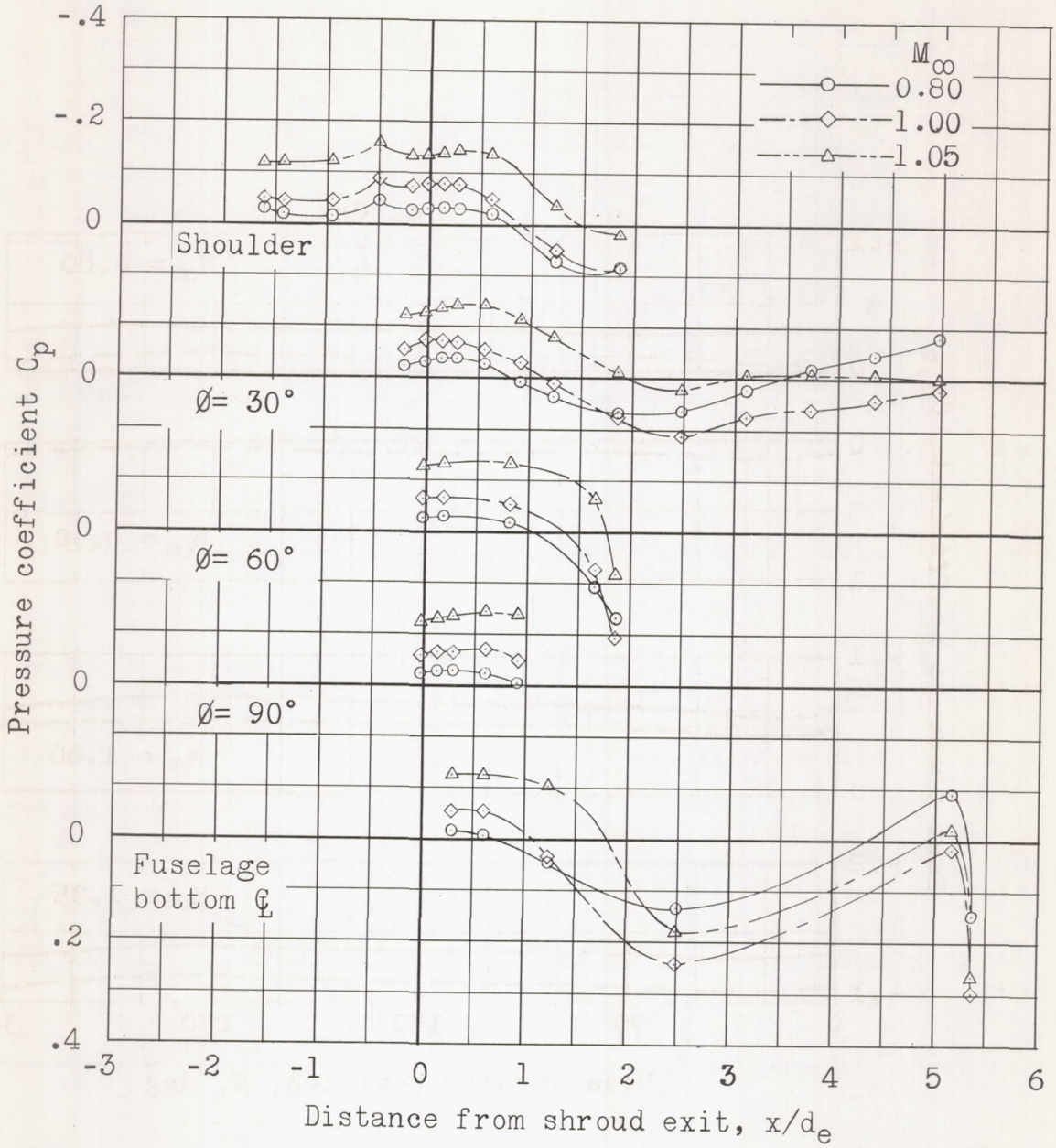

(a) $\alpha = 0^\circ$.

Figure 14.- Pressure distributions along afterbody of model with boattail area contouring. Jets off.

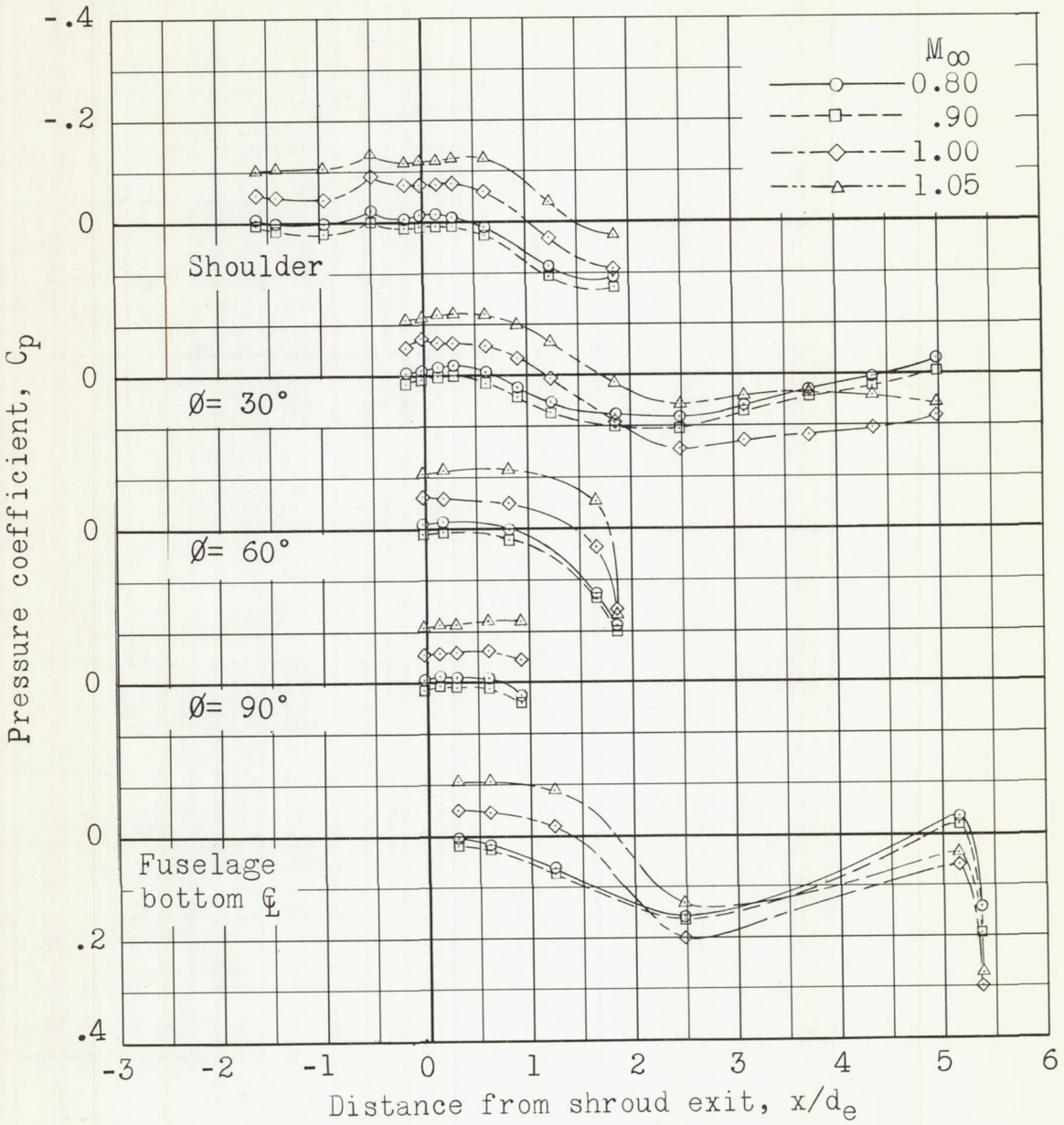

(b) $\alpha = 4^\circ$.

Figure 14.- Concluded.

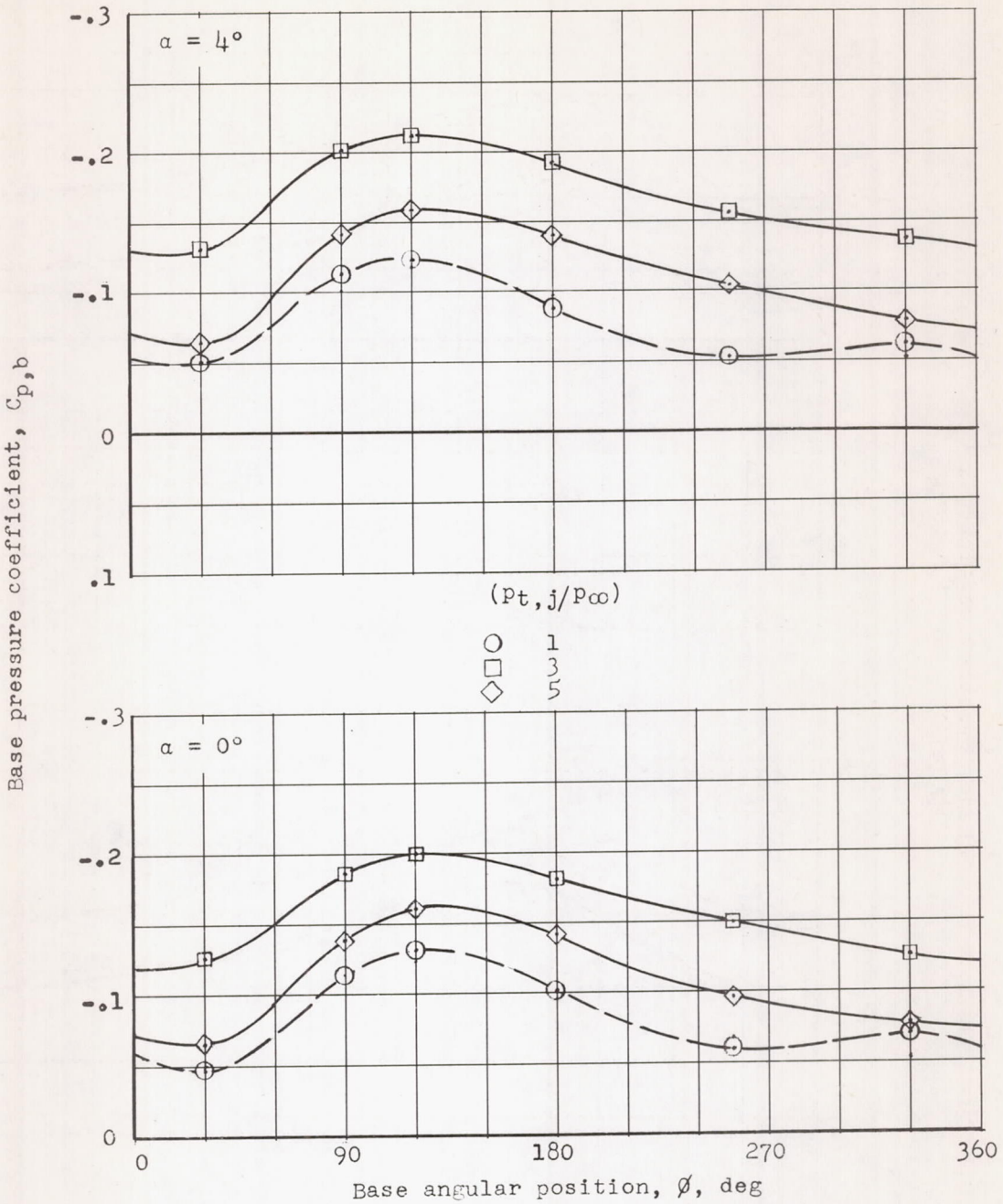

(a) $M_\infty = 0.80$.

Figure 15.- Effect of jet pressure ratio on base pressure coefficient variation around shroud annulus of basic model.

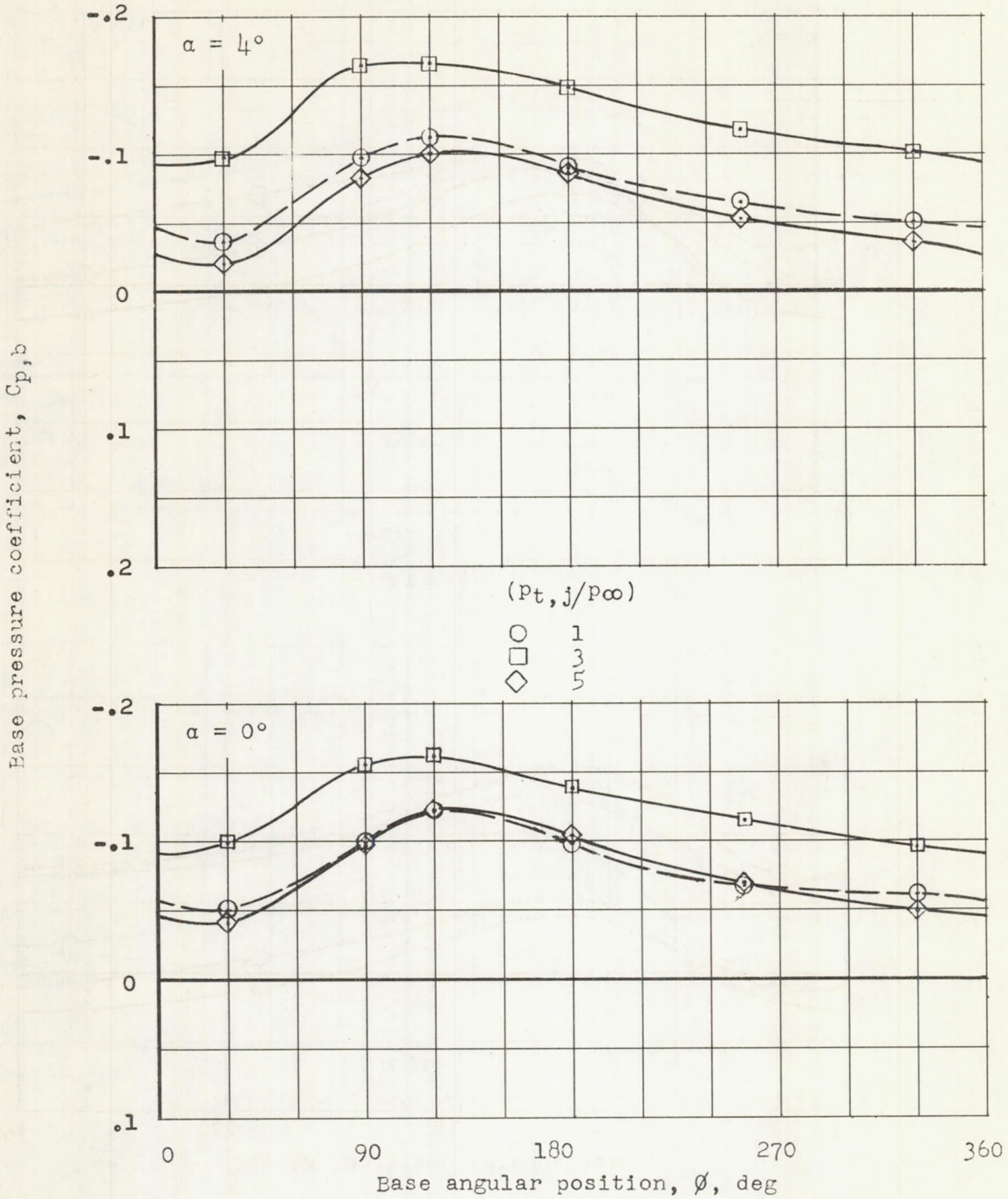

(b) $M_\infty = 0.90$.

Figure 15.- Continued.

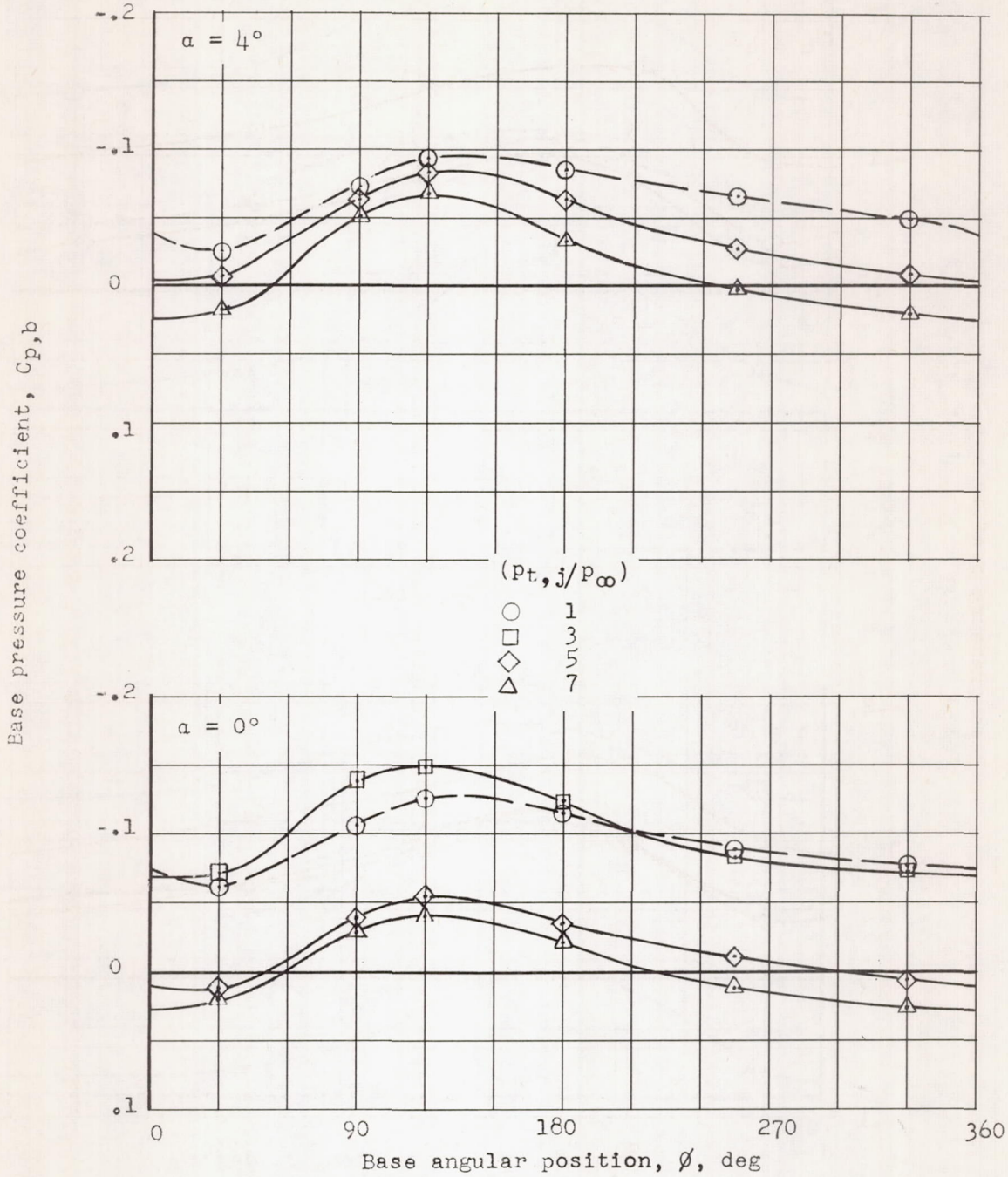

(c) $M_\infty = 1.00$.

Figure 15.- Continued.

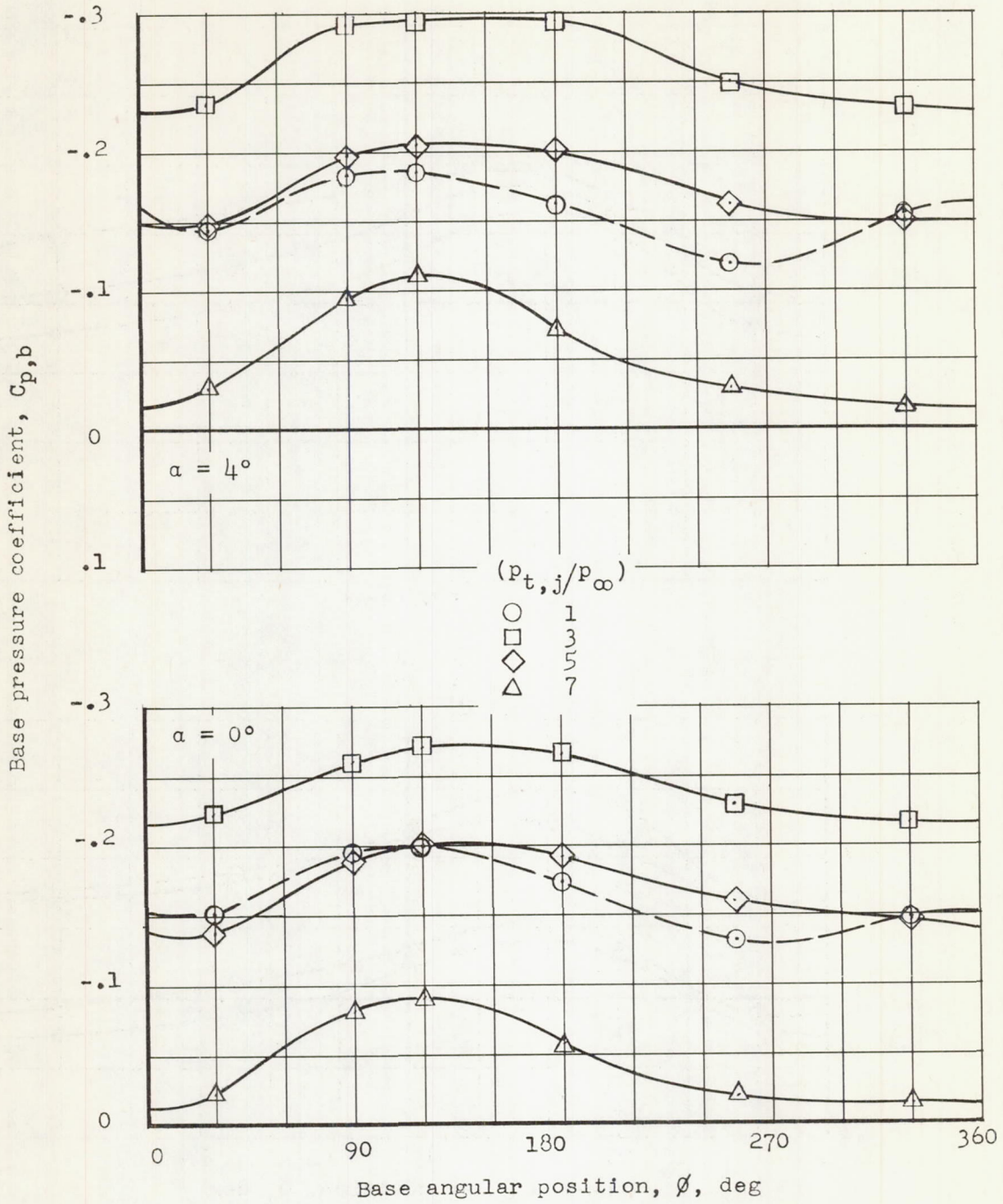

(d) $M_\infty = 1.05$.

Figure 15.- Concluded.

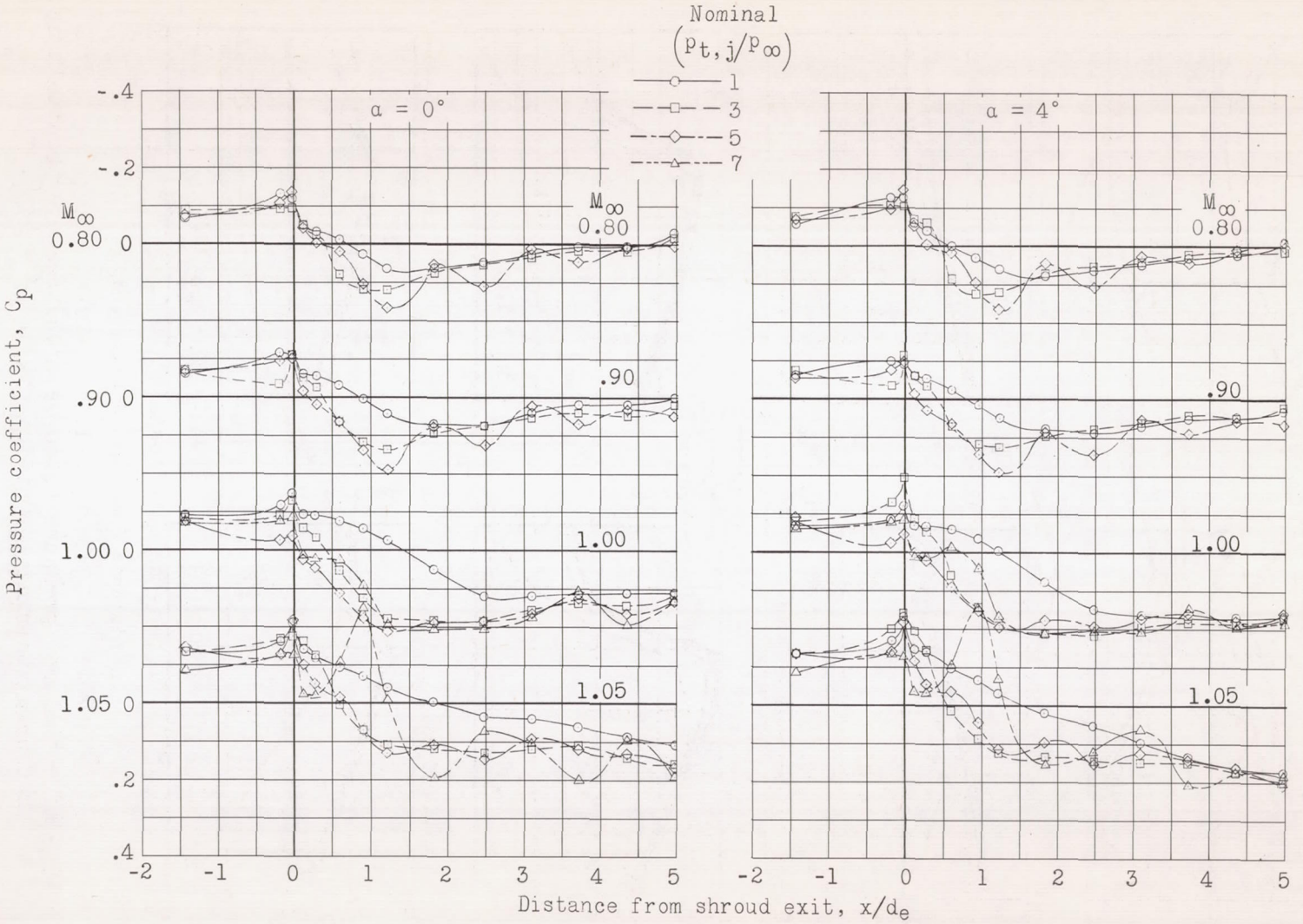

Figure 16.- Effect of jet pressure ratio on afterbody pressure of basic model. Orifice row at $\phi = 30^\circ$.

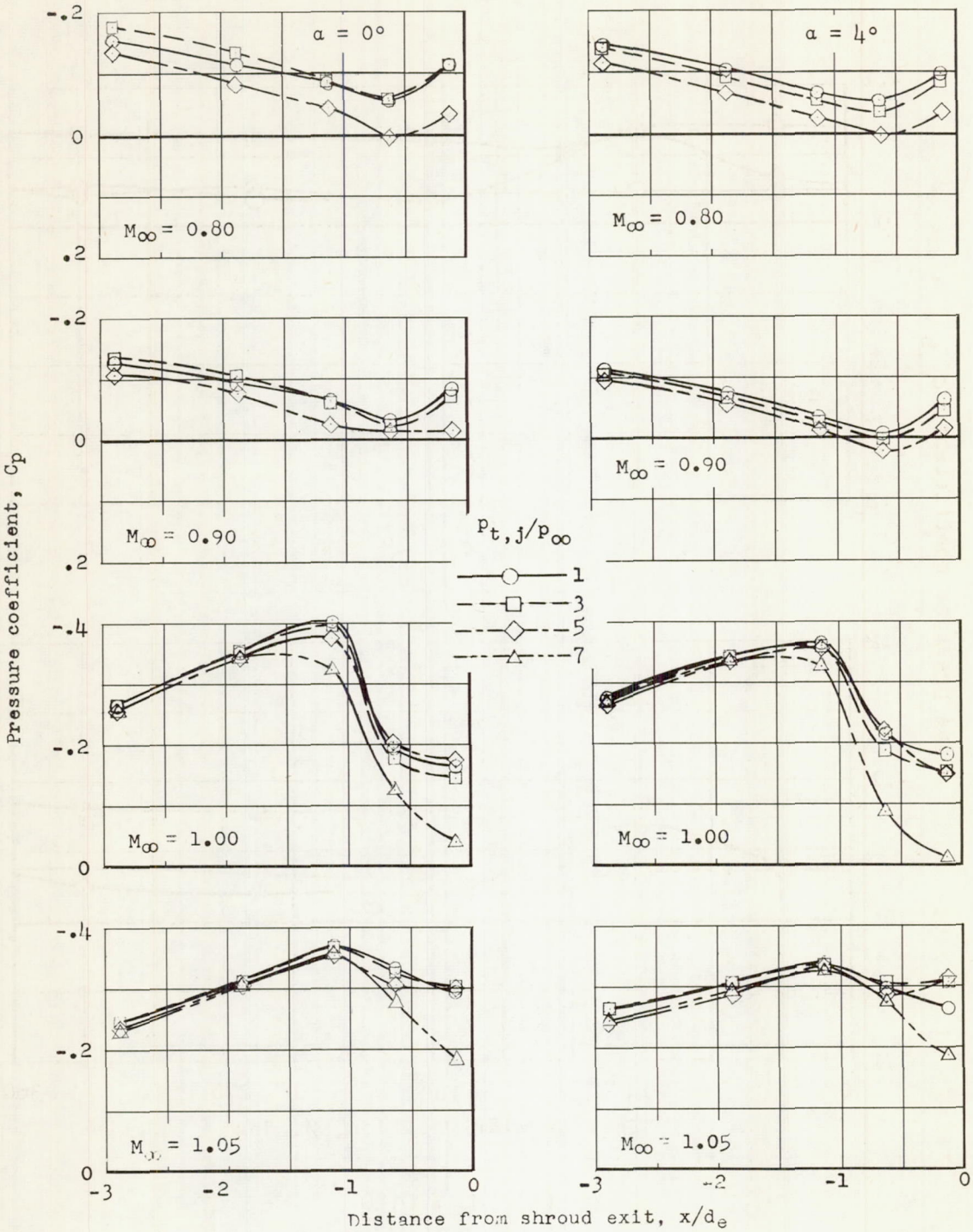

Figure 17.- Effect of jet pressure ratio on pressures over boattail area contouring fairings. Orifice row at $\phi \approx 235^{\circ}$.

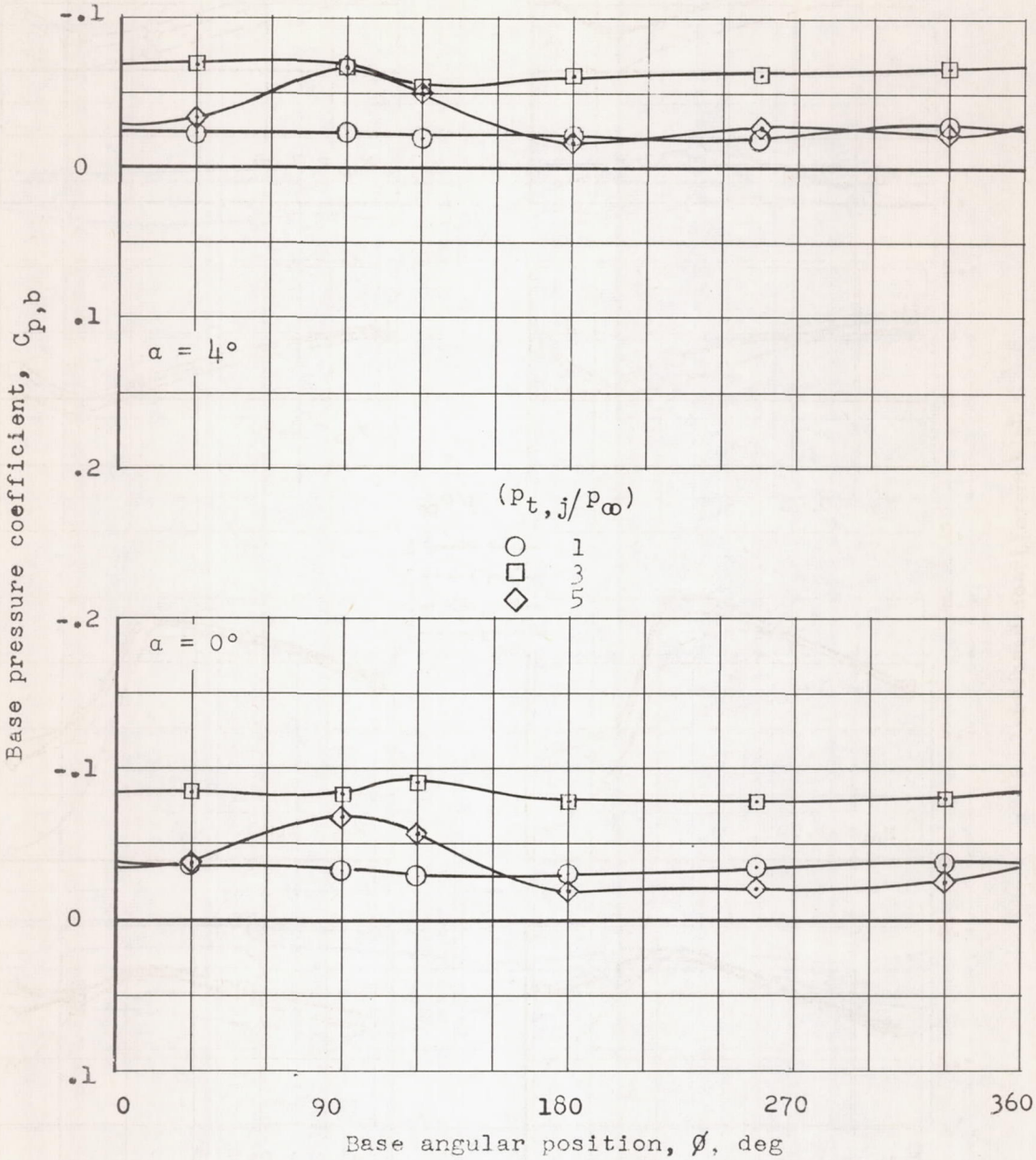

(a) $M_\infty = 0.80$.

Figure 18.- Effect of jet pressure ratio on base pressure coefficient variation around shroud annulus of model with boattail area contouring.

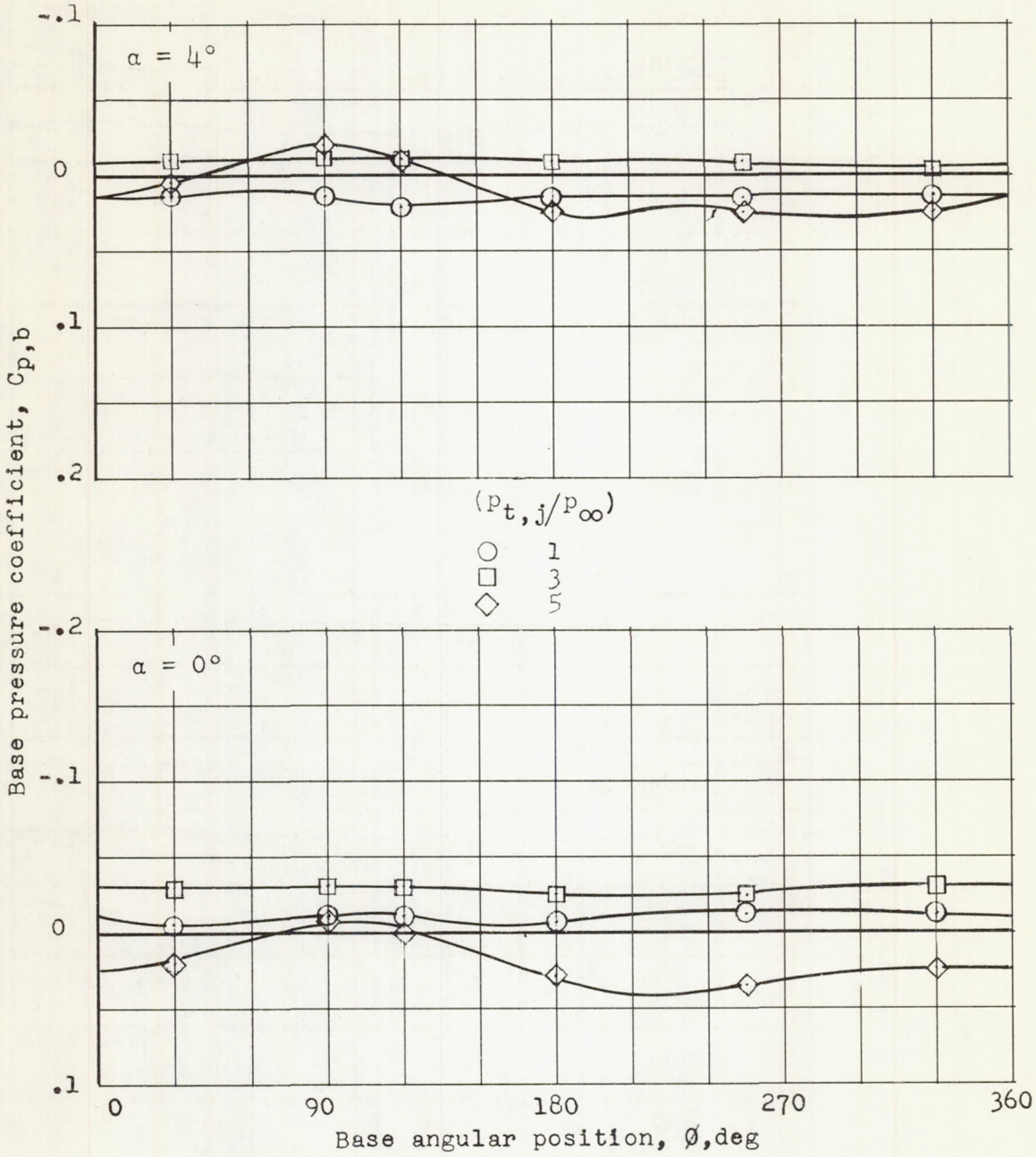

(b) $M_\infty = 0.90$.

Figure 18.- Continued.

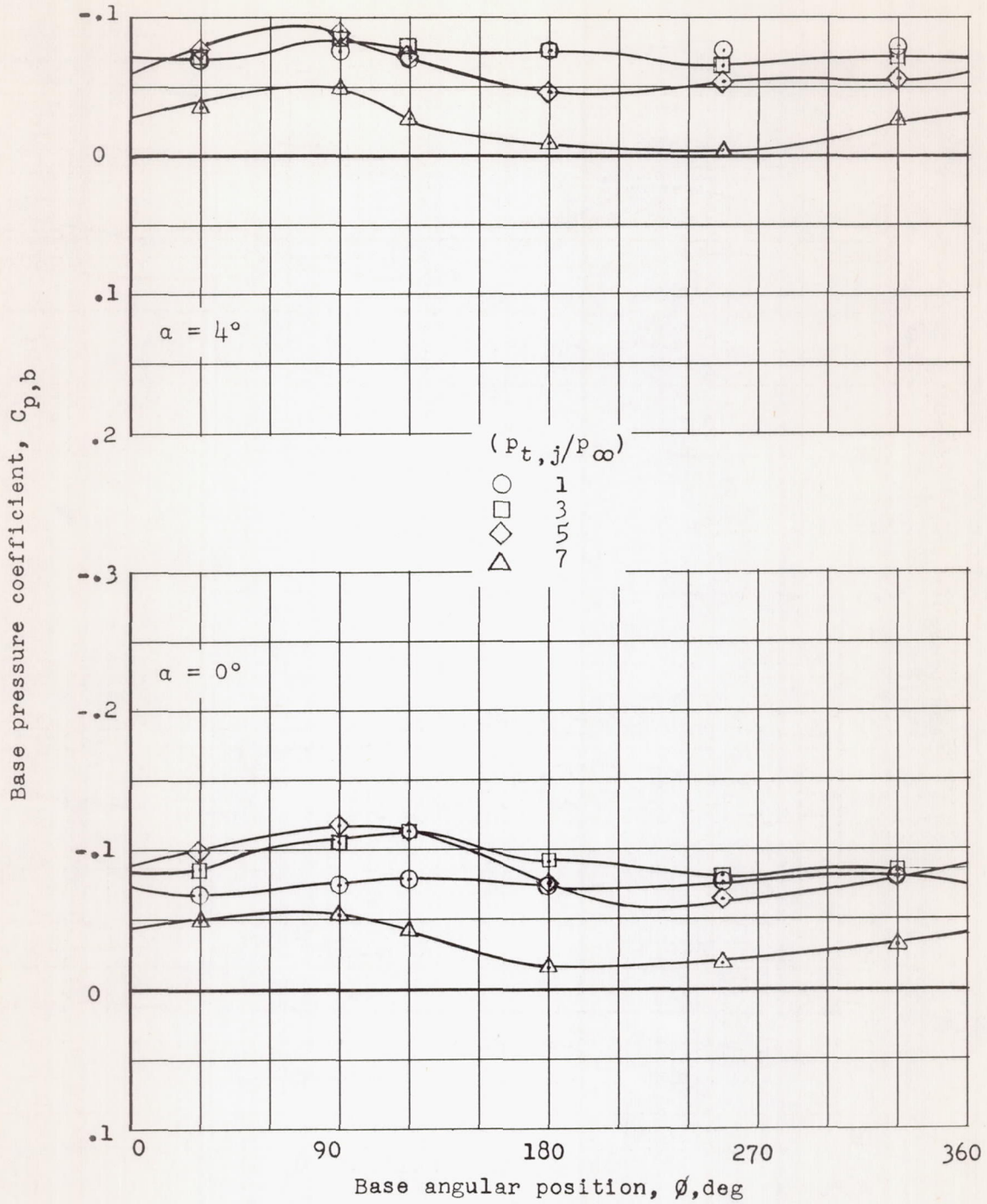

(c) $M_\infty = 1.00$.

Figure 18.- Continued.

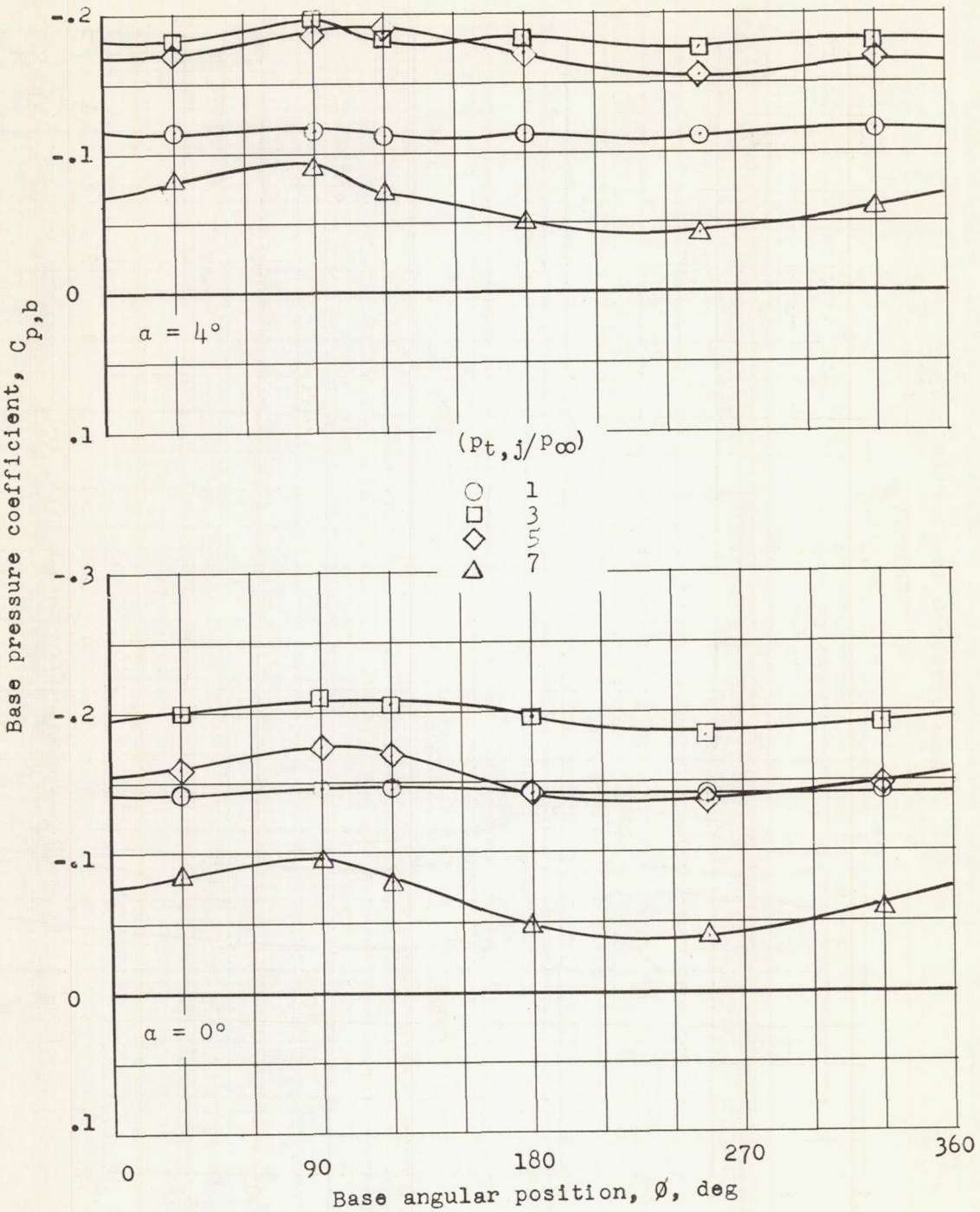

(d) $M_\infty = 1.05$.

Figure 18.- Concluded.

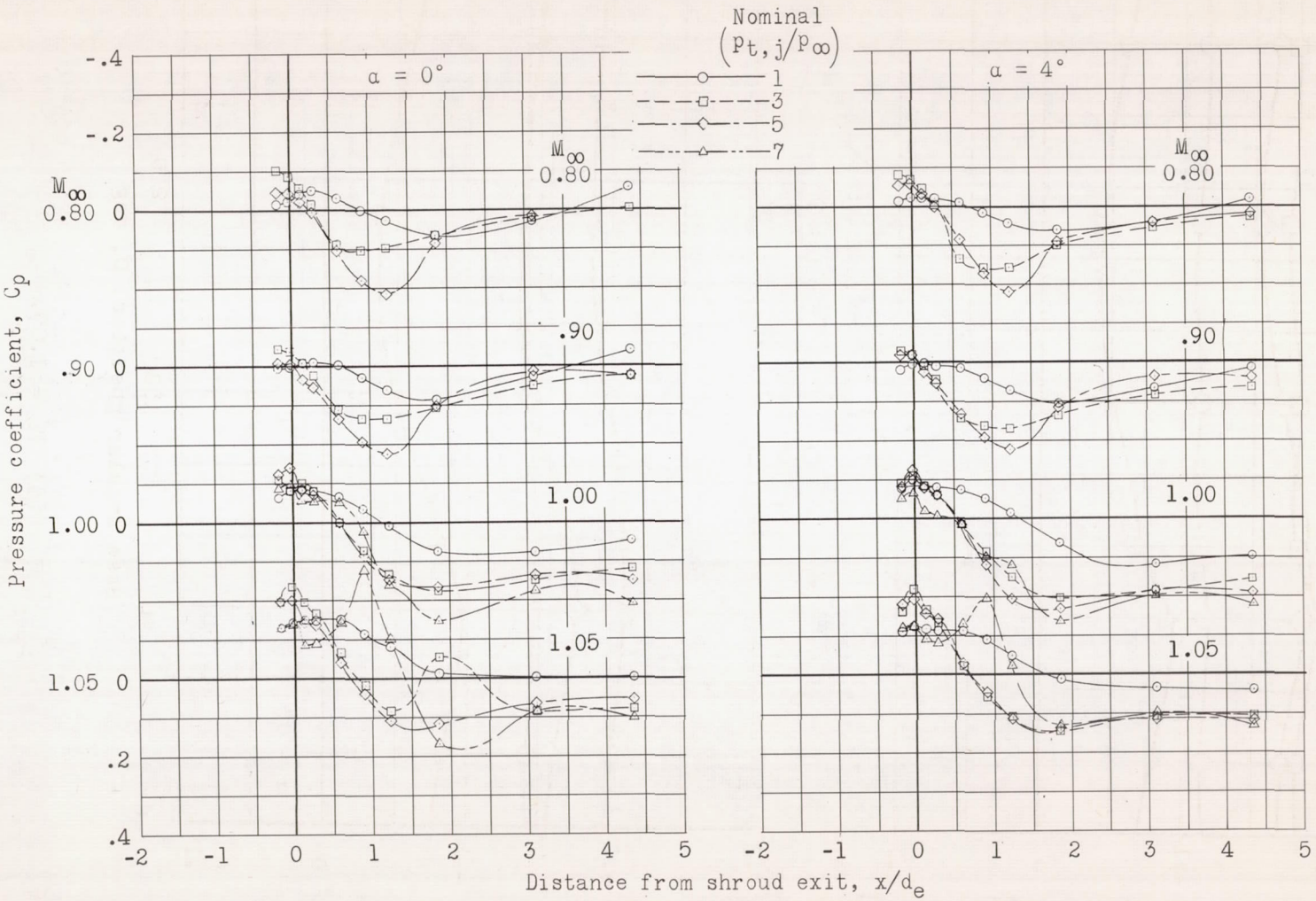

Figure 19.- Effect of jet pressure ratio on afterbody pressures of model with boattail area contouring. Orifice row at $\phi = 30^\circ$.

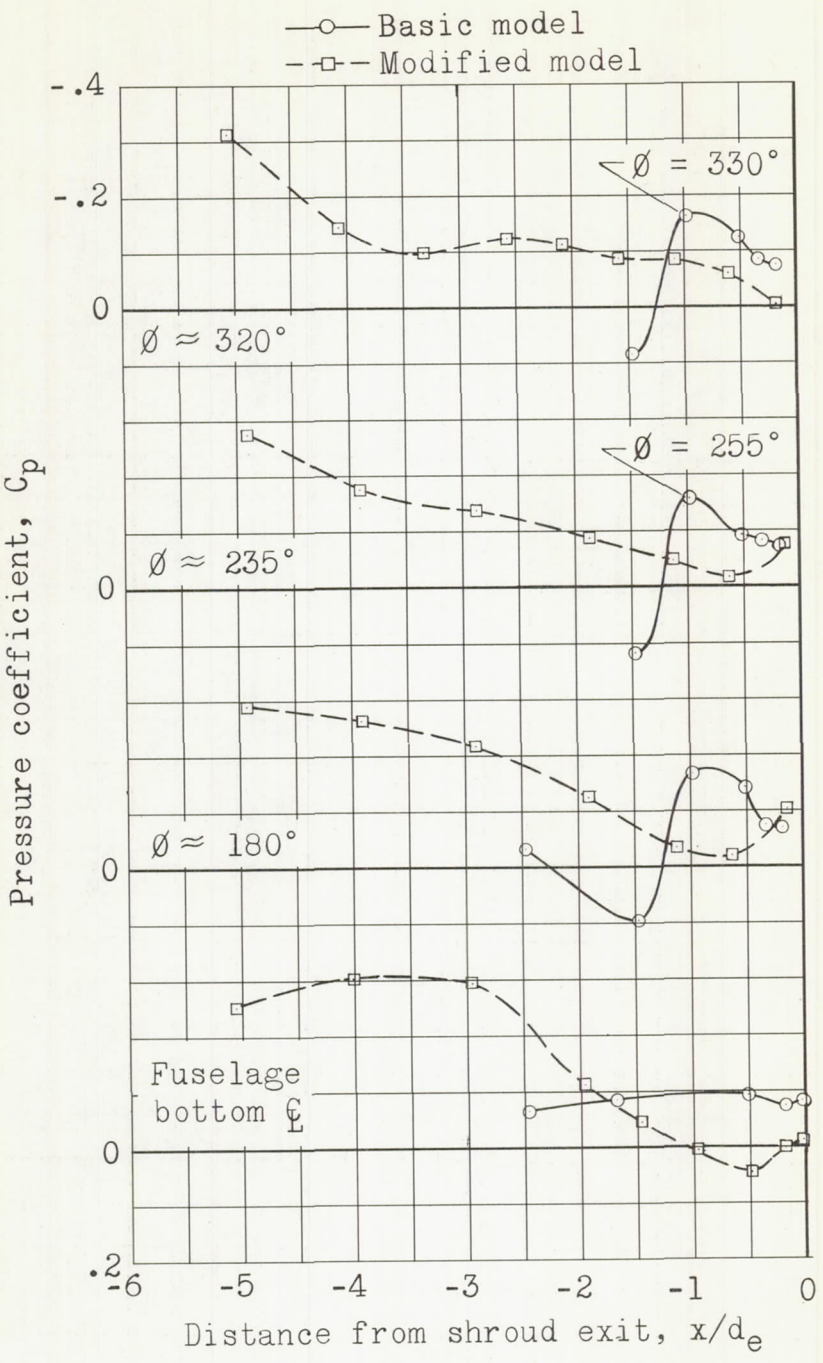

Figure 20.- Comparison of pressure distributions along boattail area contouring fairings and on basic engine shroud. $M_\infty = 0.85$; $\alpha = 4^\circ$; $\left(p_{t,j}/p_\infty\right) \approx 2.7$.

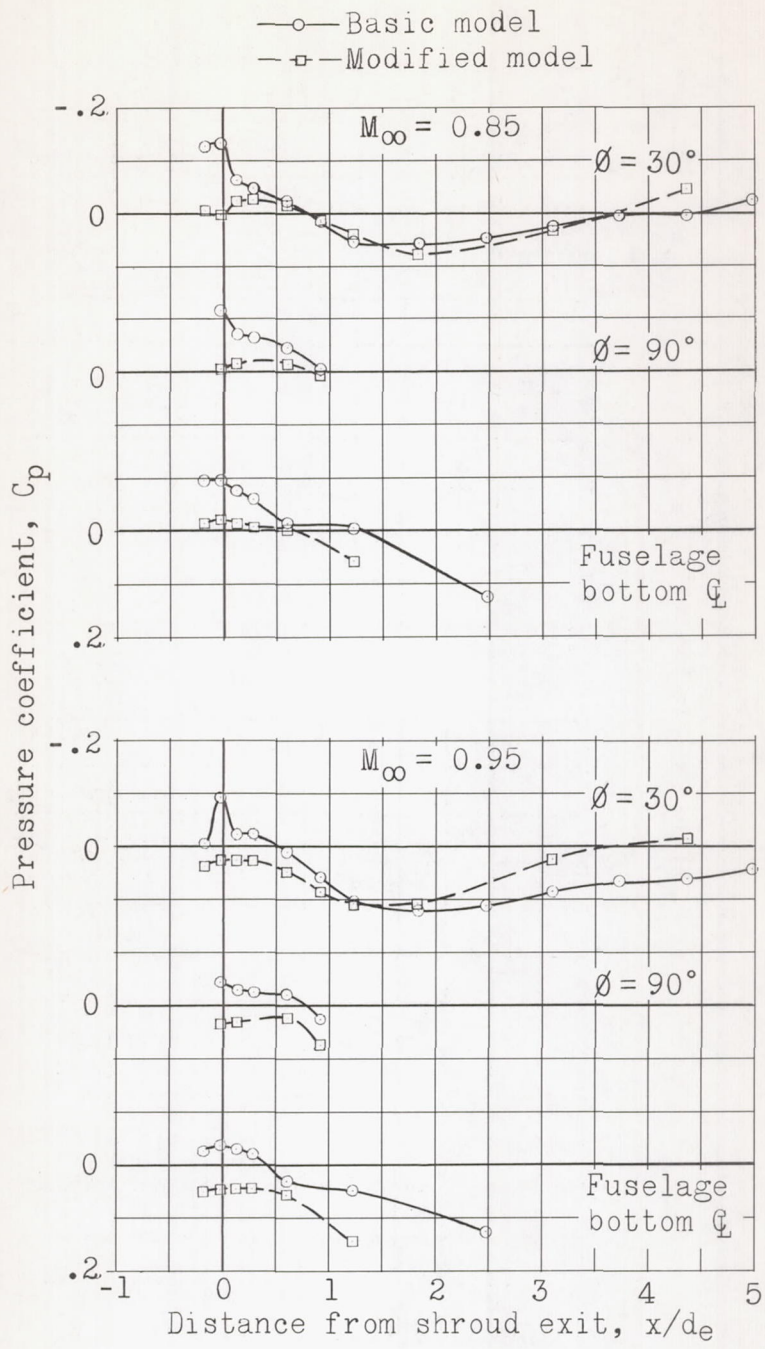

(a) $\left(p_{t,j}/p_\infty\right) = 1.$

Figure 21.- Comparison of afterbody pressure distributions for basic model and model modified with boattail area contouring. $\alpha = 0^\circ$.

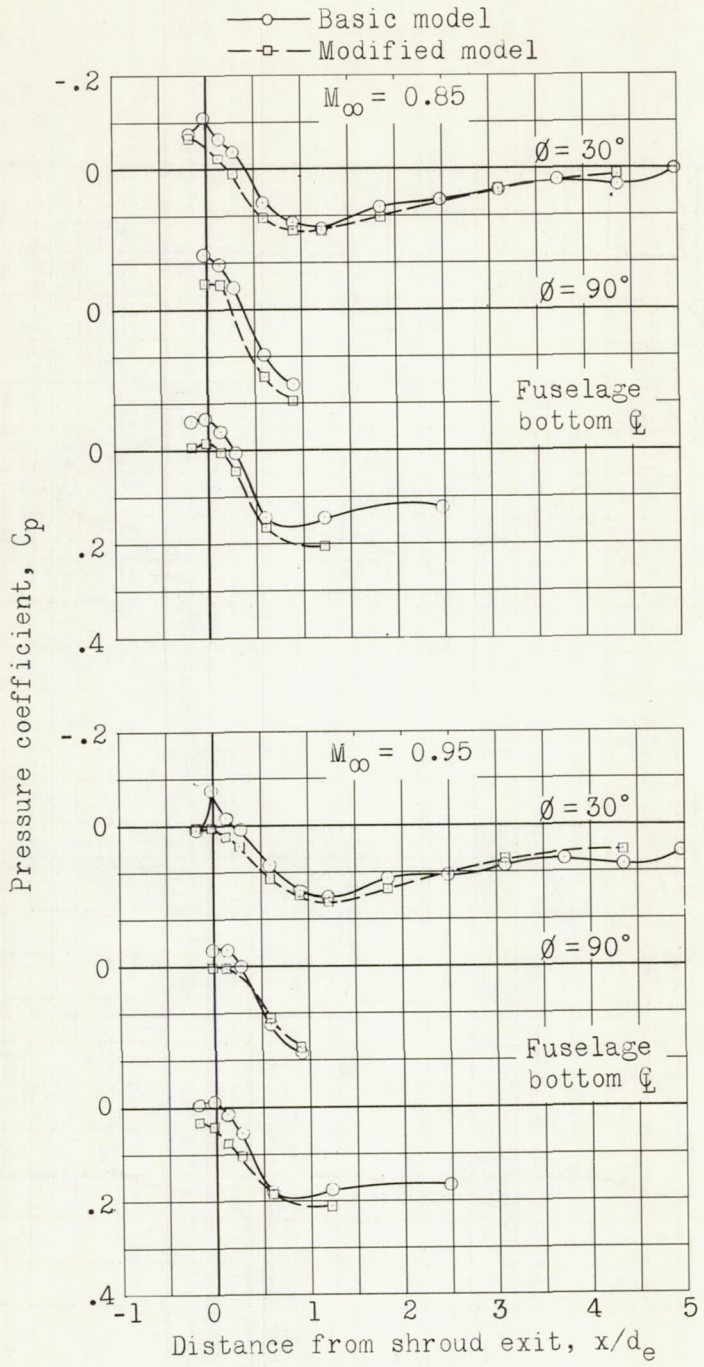

(b) $\left(p_{t,j}/p_\infty\right) \approx 3.$

Figure 21.- Concluded.

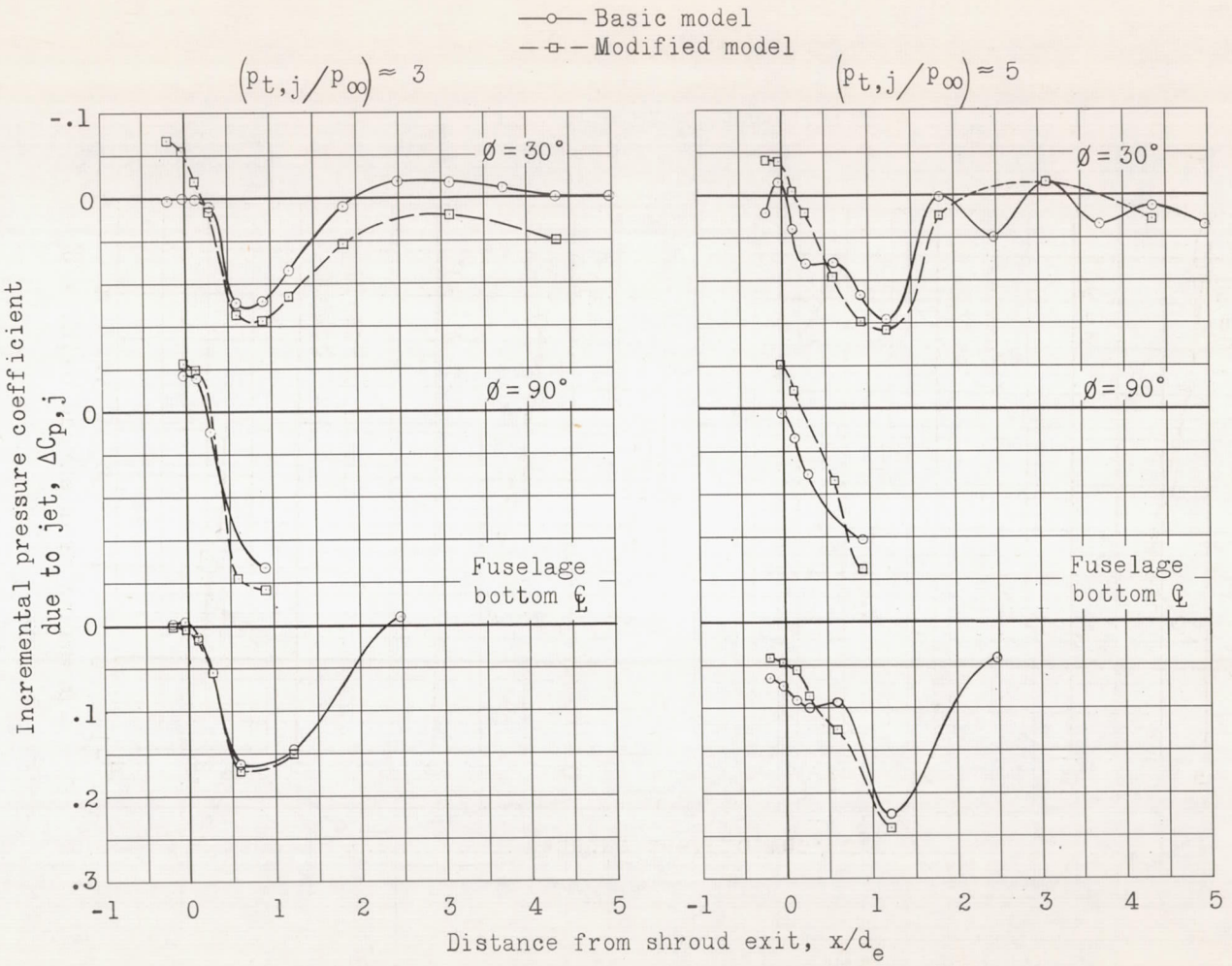

(a) $M_\infty = 0.85$.

Figure 22.- Incremental effect of jets on afterbody pressures. $\alpha = 4^\circ$.

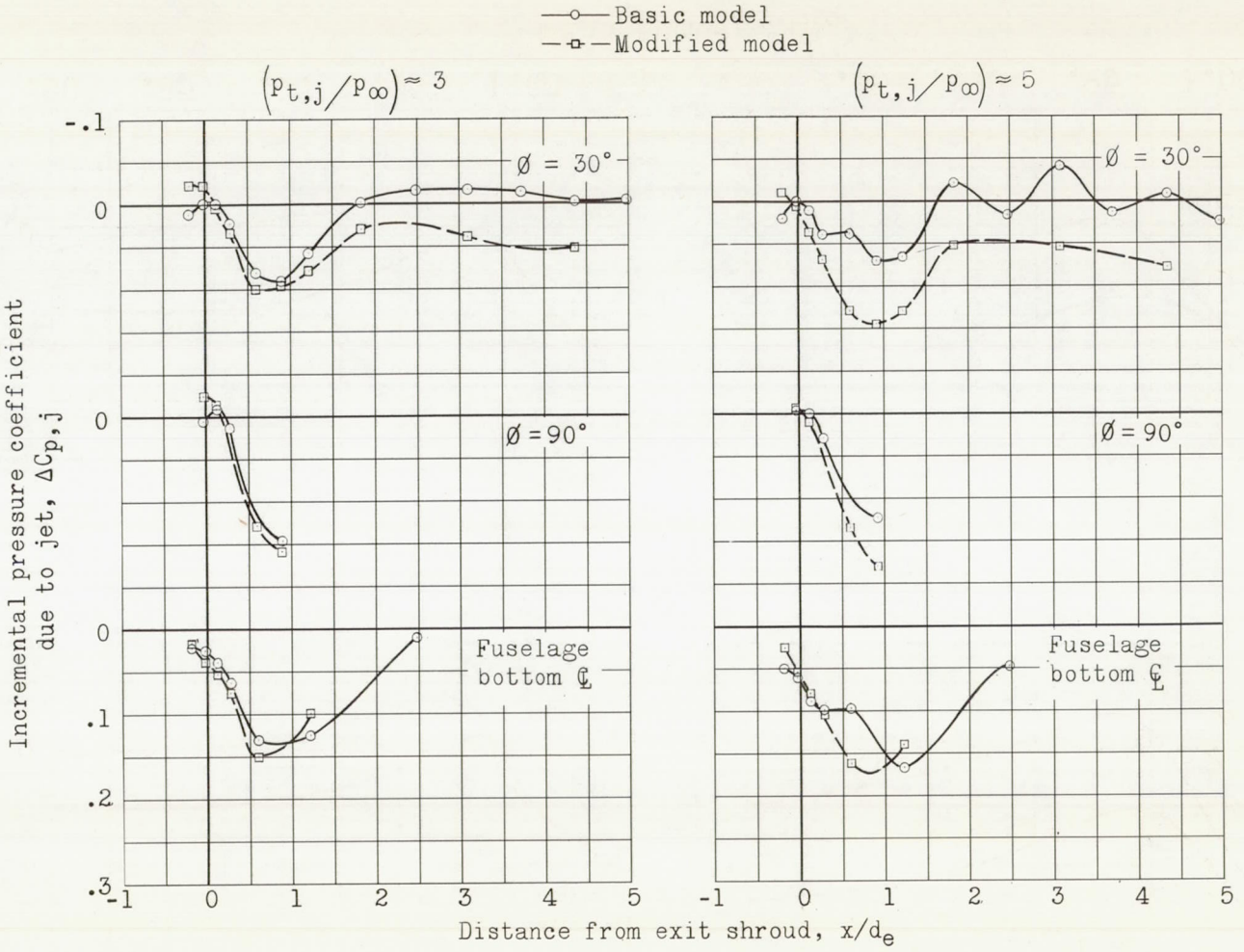

(b) $M_\infty = 0.95$.

Figure 22.- Concluded.

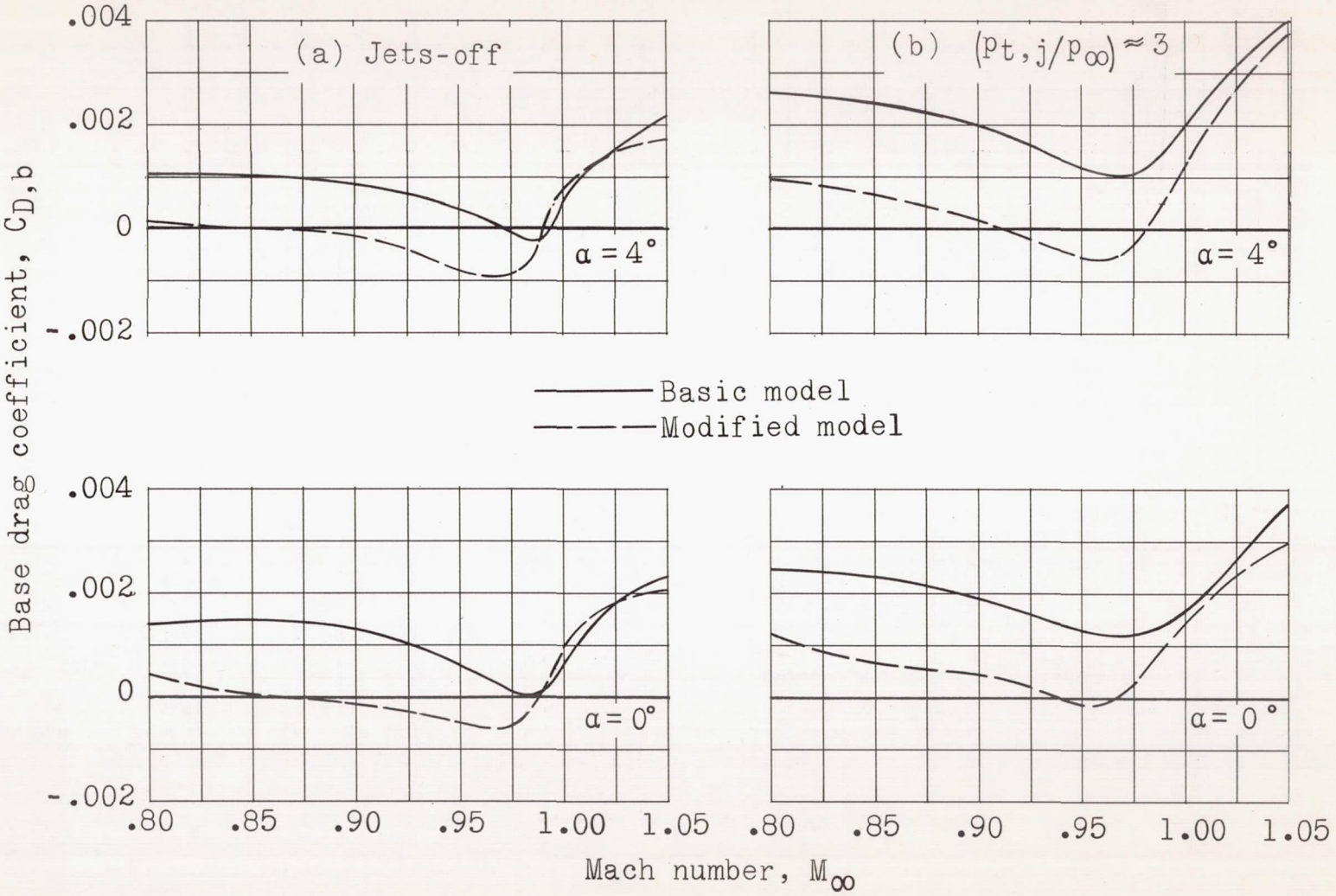

Figure 23.- Variation of base drag coefficient with Mach number for basic model and model with boattail area contouring.

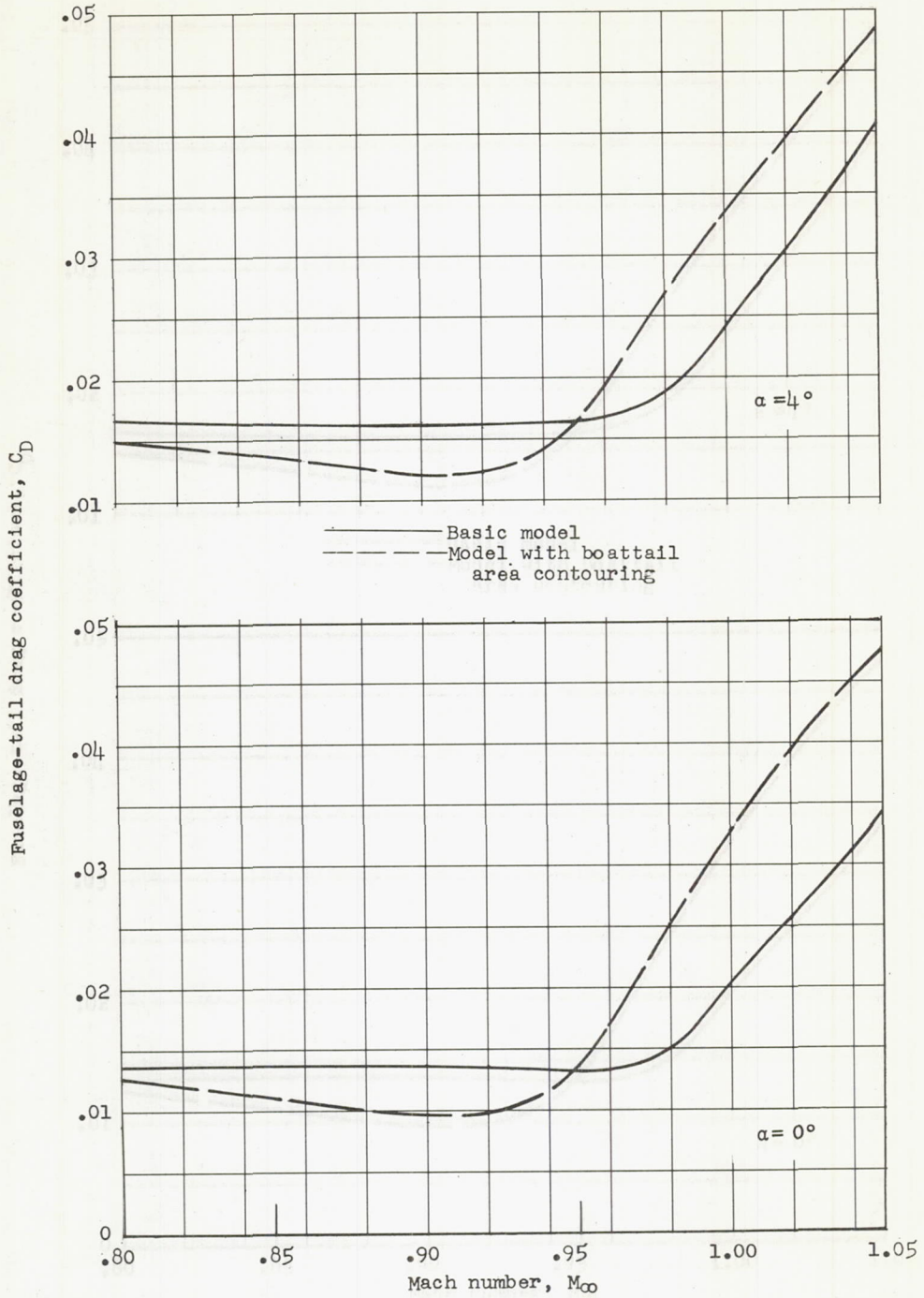

Figure 24.- Variation of fuselage-tail drag coefficient with Mach number for basic model and model with boattail area contouring. Jets off.

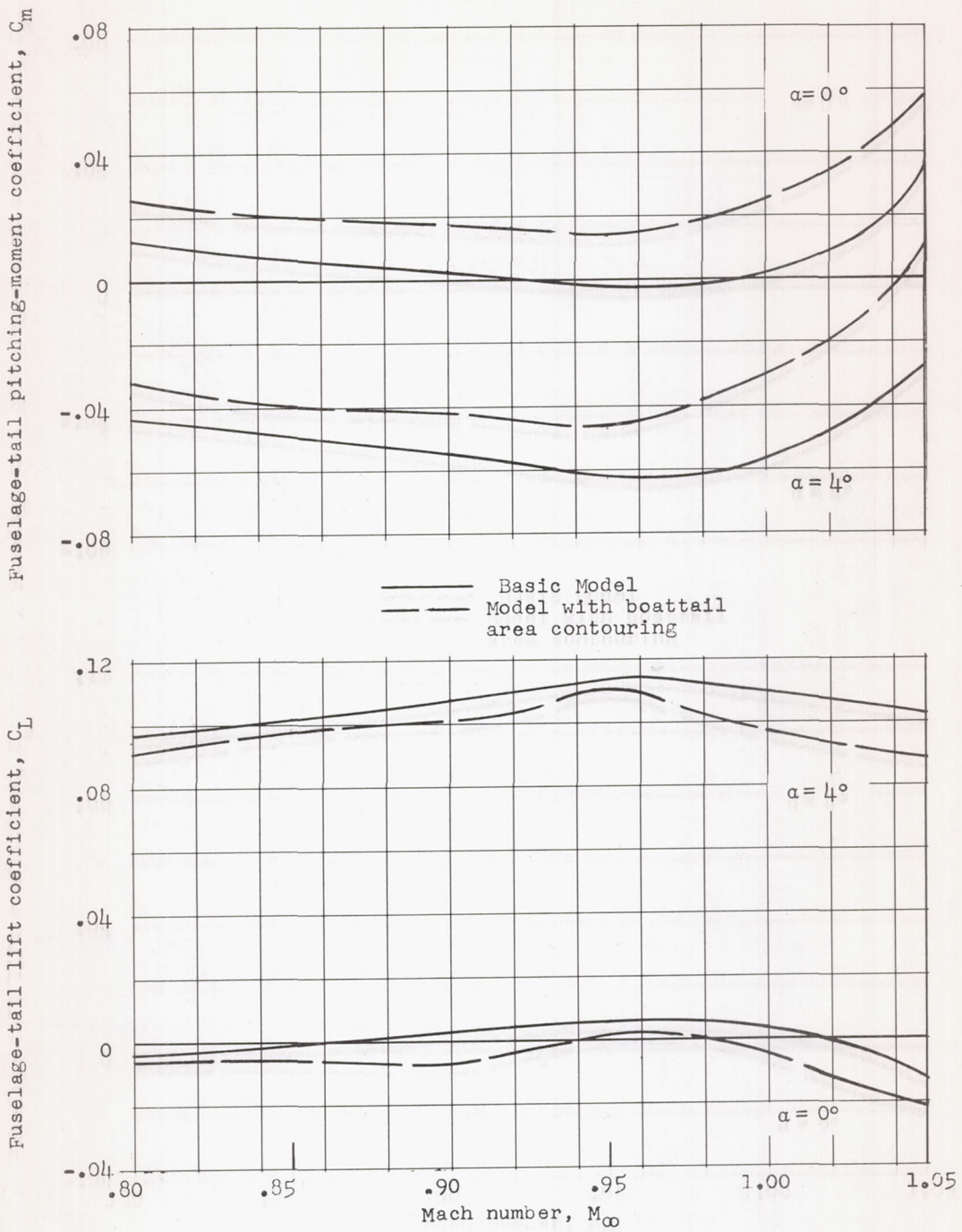

Figure 25.- Variation of fuselage-tail lift coefficient and pitching-moment coefficient with Mach number for basic model and model with boattail area contouring. Jets off.

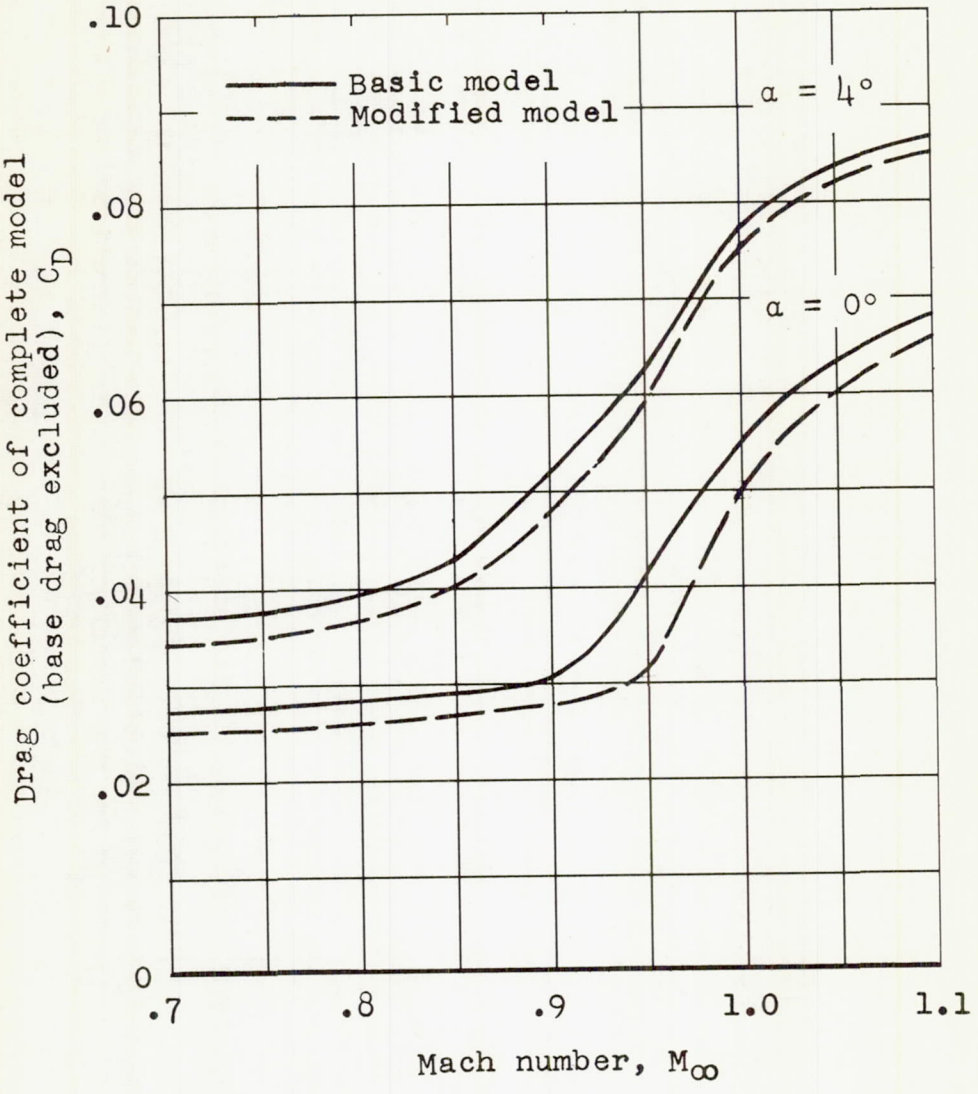

Figure 26.- Variation with Mach number of drag coefficient of complete models similar to those of present investigation. Data obtained from Wright Air Development Center 10-foot transonic wind tunnel.

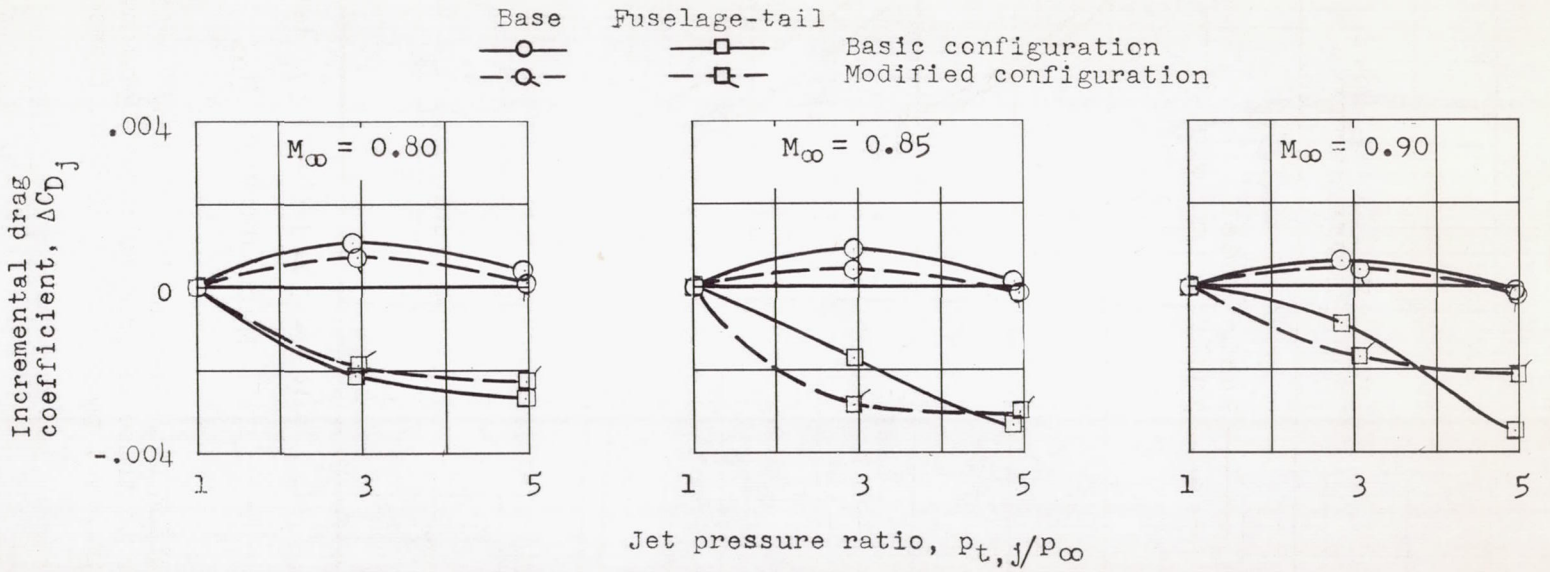

Figure 27.- Variation with jet pressure ratio of the incremental drag coefficients due to jet operation for the basic and modified configurations. $\alpha = 0^\circ$.

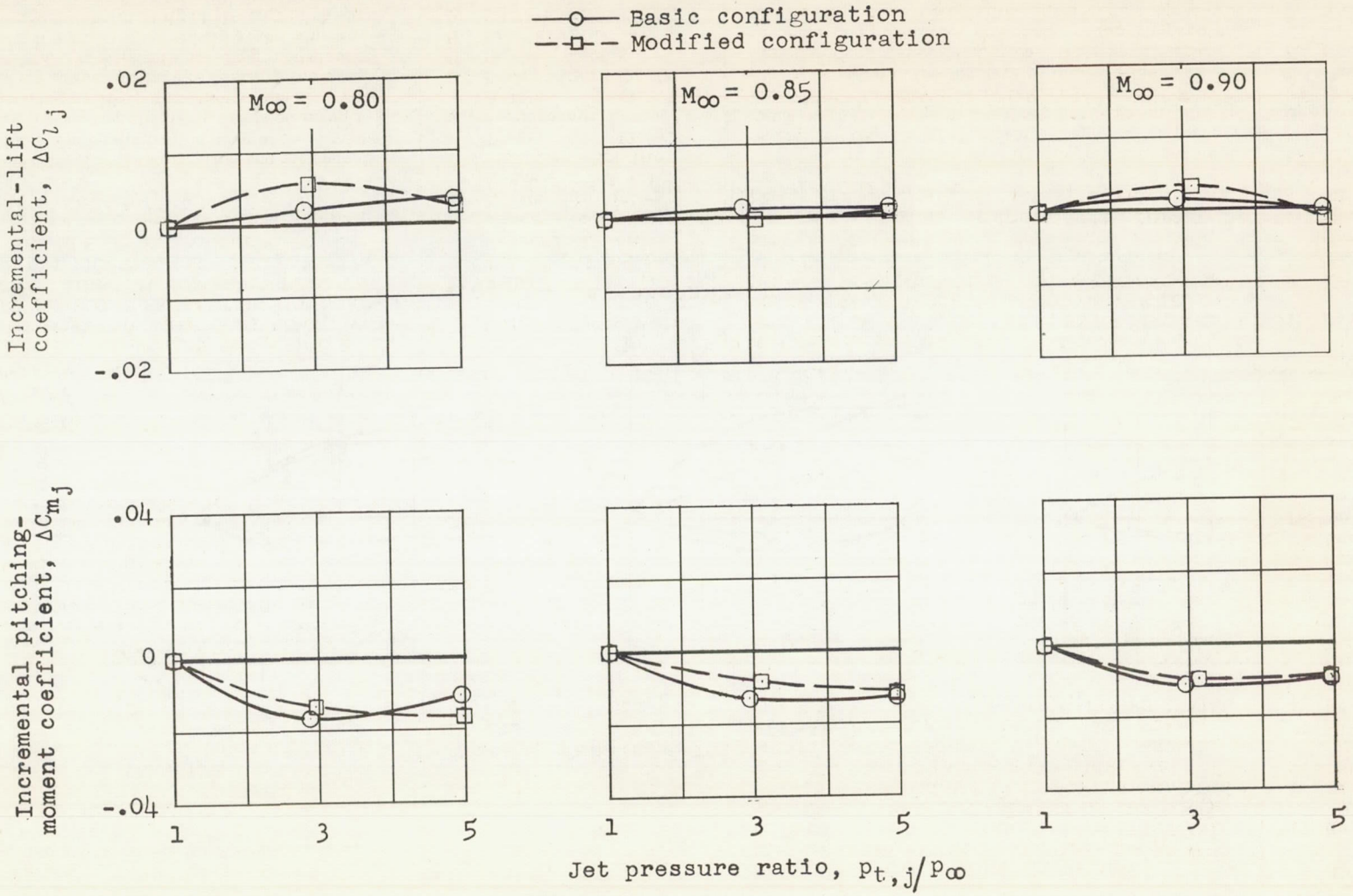

Figure 28.- Variation with jet pressure ratio of the incremental lift and pitching-moment coefficients due to jet operation for the basic and modified configurations. $\alpha = 4^\circ$.